SYNTHESIS OF ZIRCONIA NANOPOWDERS FROM LOCAL ZIRCON SAND AND INFLUENCE OF CRYSTAL STRUCTURE ON PHOTOCATALYTIC ACTIVITY

By

Mahbuba Sultana

A thesis submitted in partial fulfillment of

the requirements for the degree of

MASTER OF SCIENCE IN MATERIALS AND METALLURGICAL ENGINEERING

Department of Materials and Metallurgical Engineering

BANGLADESH UNIVERSITY OF ENGINEERING AND TECHNOLOGY

Dhaka-1000, Bangladesh

July, 2022

i

The thesis titled 'SYNTHESIS OF ZIRCONIA NANOPOWDERS FROM LOCAL ZIRCON SAND AND INFLUENCE OF CRYSTAL STRUCTURE ON PHOTOCATALYTIC ACTIVITY' submitted by Mahbuba Sultana Roll No: 0417112007 Session April/2017 has been accepted as satisfactory in partial fulfilment of the requirement for the degree in Master of Science in Materials and Metallurgical Engineering on 3rd July 2022.

Board of Examiners

1. *Fahmida*

Dr. Fahmida Gulshan   Chairman

Professor   (Supervisor)

Department of MME, BUET, Dhaka

2. _____ M.HASAN _____

Head/Director   *Dr. Mahbub Hasan*   Member

Professor   (Ex-Officio)

Department of MME, BUET, Dhaka

3. *Rashed*

Dr. Hossain Mohammad Mamun Al Rashed   Member

Associate Professor

Department of MME, BUET, Dhaka

4. *BM*

Dr. Md. Muktadir Billah   Member

Associate Professor

Department of MME, BUET, Dhaka

5. _____

Dr. Al-Nakib Chowdhury   Member

Professor   (External)

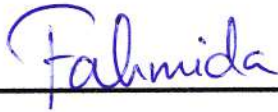Department of Chemistry, BUET, Dhaka

CANDIDATE'S DECLARATION

This is to certify that the work presented in this thesis is original and this thesis or any part of it has not been submitted elsewhere for the award of any degree or diploma.

Mahbuba Sultana

i

CERTIFICATE OF RESEARCH

This is to certify that the work presented in this thesis is carried out by the author under the supervision of Professor Dr. Fahmida Gulshan, Department of Materials and Metallurgical Engineering, Bangladesh University of Engineering and Technology, Dhaka.

Dr. Fahmida Gulshan

Mahbuba Sultana

Acknowledgement

Dedicated to my beloved kids (Yameen and Zayeem) …………..

Abstract

In the present study purification of natural zircon sand was performed by hydrometallurgical method and zirconia (ZrO_2) nanopowders were synthesized from the purified zircon. Later influence of crystal structure on photocatalytic activity was investigated. The characterization and upgradation processes were employed on local $ZrSiO_4$ sand collected from Cox's Bazar Sea Beach via Beach Sand Minerals Exploitation Center (BSMEC). Traditional beneficiation methods like acid leaching and alkali leaching were performed. As received sample contained 73.8% $ZrSiO_4$ which turned 86.3% purity after upgradation. Major impurity rutile (19.8%) was removed completely through these beneficiation processes. The particles found uniformly distributed and possessed negligible amount of moisture. Standard tetragonal phase of $ZrSiO_4$ was found in the as received sample which didn't show any phase transition at low temperature (up to $750^{o}C$). Through consecutive alkali-fusion, co-precipitation followed by calcination ZrO_2 nanoparticle with different phases were formed from $ZrSiO_4$ nano powder. Depending on calcination temperature ZrO_2 showed different crystal structure. Calcination at $800^{o}C$ and $1000^{o}C$ showed predomination of tetragonal ZrO_2 whereas comparatively high temperatures ($1100^{o}C$ and $1300^{o}C$) showed mostly monoclinic structure. Zirconia samples with different crystal structures were used to decolorize Methylene Blue dye. Calcined sample at $1100^{o}C$ showed maximum decolorization (71.75%) efficiency due to presence of combined monoclinic, cubic and tetragonal phases. The result concludes that nanoparticle of zirconia can be synthesized from local zircon sand and it can be used for photodegradation of textile dye.

Table of Contents

Chapter 5 Conclusion 79

References 83

Nomenclature

XRF	X-ray fluorescence
XRD	X-ray Diffraction
TGA	Thermo Gravimetric Analysis
SEM	Scanning Electron Microscopy
EDS	Energy Dispersive X-ray Spectroscopy
BSMEC	Beach Sand Minerals Exploitation Center
PPM	Parts per million
RPM	Revolution per minute
Zr	Zirconium
$ZrSiO_4$	Zircon
ZrO_2	Zirconia
ZrO_2	Baddeleyite (Monoclinic ZrO_2)
MB	Methylene Blue

List of Tables

List of Figures

Introduction

1.1 Purpose of the work

Zircon is a natural combination of zirconium oxide (ZrO_2) and silica (SiO_2) which occurs accessory mineral in silica rich igneous rocks like granite, pegmatite, nepheline syenite etc. It is commonly obtained as by product in mining and processing of heavy minerals sand like rutile, garnet and ilmenite. It is also found concentrated with heavy minerals e.g., rutile, in river and beach sands [1]. The main mineral precursor of ZrO_2 production is $ZrSiO_4$ sand. Zircon is one of the most important heavy minerals occurring in the beach sand along the coast of Bangladesh. Research found that the reserve of zircon in Bangladesh is about 158,117 thousand ton [2]. Removal of unwanted impurities present in zircon sand is a complex process. Hydrometallurgical routes are found to be good processes for removal of unwanted elements and synthesize of nearly pure zircon.

In general, nanomaterials exhibit unique properties due to their miniature size. The approaches for fabricating nanoparticles can be classified into top-down and bottom-up methods. The former method changes the material from an initial size of a few micrometers into one of nanometers [3]. Present nano-size zircon was produced by dry ball mill which was a top-down technique. For extraction of ZrO_2 from $ZrSiO_4$ a variety of techniques have been proposed like alkali digestion, chloration, co-precipitation, reductive smelting, sol-gel, hydrothermal, ion-exchange method etc [4]. Synthesis of ZrO_2 by alkali fusion followed by co-precipitation and annealing is a promising one. This technique would help to avoid the troubles of waste disposal of solid and liquid by product [1].

It is well-known that ZrO_2 has three different polymorphs (monoclinic, tetragonal, cubic). Preparation method plays an important role in determining the final crystal structure of ZrO_2 [5]. Zirconia shows photo catalytic behavior due to presence of relatively wide band gap Eg (3.25-5.1 eV) and the high negative value of conduction band potential [6]. Though different surface properties on different zirconia polymorphs have extensively been studied, effect of crystal structure on photocatalysis has rarely been investigated. The concern of the present research work is to study the photocatalysis behavior of synthesized zirconia from local zircon sand.

The rapid growth of the textile industry has led to the accumulation of various organic pollutants with dyes accumulating in water bodies as a particularly severe example. Photocatalysis is one promising approach to protect the aquatic environment based on its ability to oxidize low concentration of organic pollutants in water [7]. ZrO_2 nanoparticle has been considered as a photo-catalyst in different chemical reactions for degradation of dye.

The objective of the present study is to synthesize nanocrystalline amorphous, tetragonal and monoclinic ZrO_2 samples from locally available purified $ZrSiO_4$ sand and after that photocatalytic degradation of methylene blue over the different ZrO_2 samples were studied.

1.2 Outline of the work

The aim of this work can be summarized as follows:

- Purification of natural zircon sand by hydrometallurgical method and synthesis of zirconia nano-powders from the purified zircon.

- Characterization of the samples on the basis of material composition and crystallinity. Also carry out study on the influence of crystal structure on photocatalytic activity.

The outline of the work is mentioned bellow:

a) **Sample Collection, Beneficiation and Synthesis**

i.   The natural zircon sand was collected from Cox's Bazar sea beach. At first it was separated by magnetic and electric separator.

ii.   As received sample was purified by hydrometallurgical route. (Acid leach and Alkali leach)

iii.   The pure zircon powder was synthesized by top-down method which converts into zircon nano-powder via dry ball milling.

iv.   Zirconia nano powder was synthesized by alkali fusion with NaOH at $700^{o}C$, Co-precipitation of alkali fusion product by HCl and NH_4OH and finally calcination.

v.   Co-precipitated product was calcined at different temperatures to find

different crystal structure.

b)   Characterization

i.   The mineralogical composition of as received and refined samples were determined by XRF analysis.

ii.   The XRD analysis were performed to reveal the phase.

iii.   The morphology of the sand samples was studied via optical, scanning electron and polarization microscopy.

c)   Evaluation of photo catalytic activities

i.   Zirconia powder was added as photo-catalyst to dye solution and the suspension was subjected to UV irradiation. The decolorization efficiency of the zirconia powder was determined by using a UV-Visible Spectrometer.

ii.   The influence of crystal structure on photo catalytic activity was studied.

1.3   Structure of the thesis

This book contains total five chapters which are the introduction, literature review, experimental procedure, results and discussion and finally the conclusion.

Chapter one shows the purpose of the work. Then it elaborates the aim and objective of the work. This chapter concludes with structure of the thesis.

Chapter two discusses the review of previous related works in this thesis work. It accommodates overview of zircon and zirconia, their crystal structures, properties, applications. Zircon reserve in Bangladesh, demand situation of zircon in the world also discussed here. Different extraction and beneficiation routes of mineral processing are explored in this chapter. Different synthesis techniques of zirconia production used by different researchers are chalked out here. Chapter two ends with a brief review on photocatalysis.

In chapter three, material selection along with different characterization procedure used in the experiment like XRF, SEM, XRD, SEM/EDS, polarizing microscopy, UV-Vis spectroscopy etc are discussed elaborately. Hydrometallurgical routes like acid and alkali leaching used in the research work are also explained here. Experimental procedure of synthesis technique of zirconia nanoparticles (alkali-fusion and co-precipitation) and evaluation of photocatalytic behavior are elaborated in this section.

In chapter four all obtained results along with explanations are summarized. Finally in chapter five conclusion has been drawn from the empirical results.

Chapter Two

Literature Review

Sand is naturally occurring loose granular material blanketing the beaches, riverbeds and deserts of the world. It is composed of finely divided rocks and mineral particles. The composition of sand is variable depending on location of rock sources and environmental conditions. It is non-renewable form of resources consists of mainly silica, calcium carbonate etc.

Zircon is found in beach sand as heavy mineral. It is one of the two core product streams from 'mineral sands', the other is titanium minerals. It can be found by processing of heavy mineral sand deposits [8].

Deposits of mineral sands are formed along ancient coastline. Weathering processes like wind, rain and freezing /thawing cycles break down heavier minerals into smaller grains and found concentrated in sea shores or riverbanks. The heavy mineral content of these sand deposits can range from .5% to >20%. Zircon content varies from deposit to deposit ranging from 1% to 50% [10].

2.1 Overview of Zircon

Zircon referred as zirconium silicate ($ZrSiO_4$) is a tetragonal crystallize structure consists of 67% zironia and 32.8% silica. Typically, zircon contains small amount of hafnium (Hf) approximately 1% [9]. The natural colour of zircon varies between colourless, yellow-golden, red, brown, blue, green and so on. Zircon varies from deposit to deposit in terms of grain size, shape and chemical purity [10]. Zircon often crystallizes in tetragonal prisms terminated with sharp, pointed, pyramidal faces. However, under certain conditions, zircon may crystallize with rounded ellipsoidal shapes (Fig. 2.1). It is believed by some investigators that the roundness of zircon particles in commercial sands probably reflects the original crystallization of the zircon particles from cooling magma rather than later alteration and attrition (Garnar, 1982) [9].

Fig 2.1: A mixture of tetragonal prism, rounded ellipsoid of zircon (ZrSiO$_4$) sand particle

Zircon is a heavy mineral and is resistive to external destructive agents like abrasion, chemical dissolution etc. It is very stable and can survive in many sedimentary cycles [11]. Although resistant to external alteration ZrSiO$_4$ may be subjected to internal modification from radiation. Thorium (Th) and uranium (U) may substitute for zirconium in the zircon crystal lattice but this alteration may not affect substantially the physical properties of zircon sand [12]. Zircon, being a nonmagnetic nonconductor, can be separated from other heavy minerals easily by utilizing specific gravity differences, differences in magnetic properties or differences in conductive properties [13].

2.1.1 Crystal Structure of Zircon

ZrSiO$_4$ is a common accessory mineral in nature, occurring in a wide variety of sedimentary, igneous, and metamorphic rocks. The chemical and physical properties of zircon and its ability to incorporate to retain trace elements are determined by its crystal structure [9]. Zircon shows tetragonal structure (Fig 2.2) which is adopted by numerous minerals and synthetic compounds with the general formula ATO$_4$, in which high field-strength T-site cations occupy isolated tetrahedra, and A-site cations occupy eight-coordinated dodecahedra structural sites [14]. Though zircon is a metamorphic rock it may changes its original structure and property due to presence of radioactive elements.
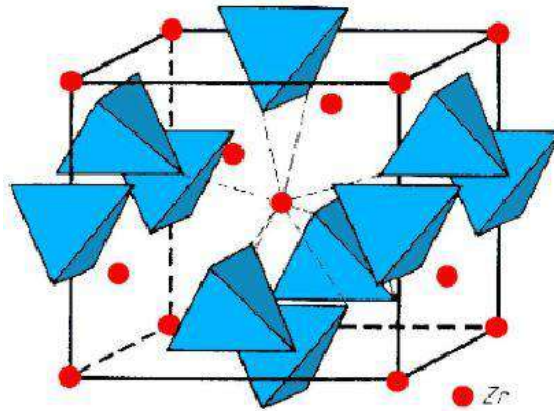
Fig 2.2: The basic tetragonal structure of zircon $ZrSiO_4$ [16]

Zircon is an orthosilicate in which isolated SiO_4 tetrahedra share corners and edges with ZrO_8 dodecahedra as shown in Fig 2.3 [15]. The ZrO_8 dodecahedra share edges with each other to form chains parallel to <100> (Fig. 2.3a) such that each ZrO_8 polyhedron shares edges with four adjacent ZrO_8 polyhedra, two in each of the crystallographically equivalent directions [100] and [010]. These <100> chains of ZrO_8 polyhedra are cross linked by sharing corners with SiO_4 tetrahedra. The Si and Zr polyhedra also form an edge-connected chain of alternating ZrO_8 and SiO_4 polyhedra parallel to [001] between which lie unoccupied channels, also parallel to [001] (Fig. 2.3b) [14,15].

The structure of zircon is relatively open, with small voids between the SiO_4 and ZrO_8 polyhedra and open channels. Such structural voids are potential interstitial sites that could incorporate impurities, provided that such sites can accommodate interstitial ions without excessive structural strain [15,16].
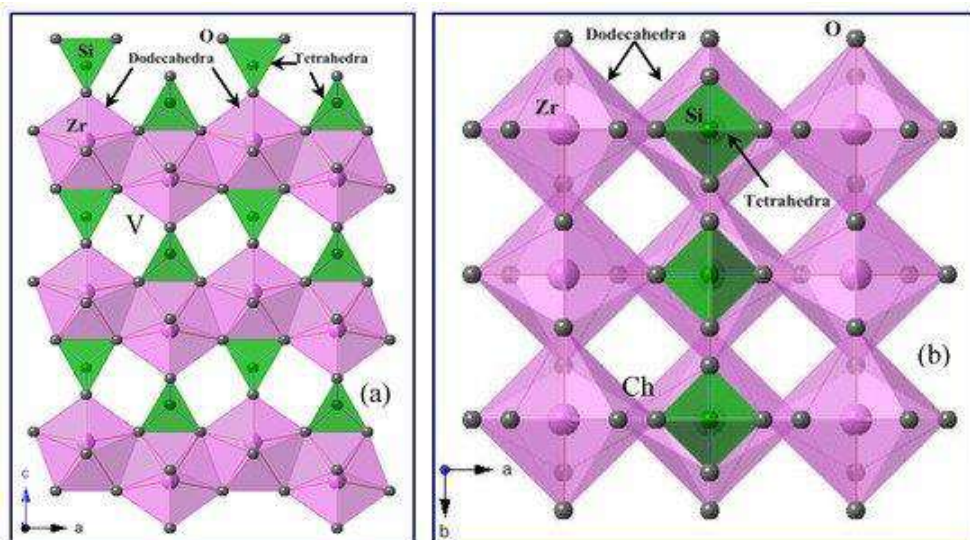
Fig 2.3: Polyhedral representation of the zircon structure, which consists of isolated SiO_4 tetrahedra and ZrO_8 dodecahedra that share their (**a**) edges with each other to form a chain parallel to **c** axis (**b**) corners with other ZrO_8 dodecahedra along the **a** and **b** axes [15]

2.1.2 Properties of Zircon

Zircon is chemically inert in nature in all conditions which turns it to mostly useable material in foundry application. It is a member of nesosilicate group and considered to be the main source of metal zirconium. Zircon is much softer than diamond and cubic zirconia and available in different colours like white and blue. Zircon has been found to be the most notable of the materials with high refractoriness, free from sudden volume changes with temperature. Other properties include good heat conduction, high strength, not easily welded in casting surface etc [17]. The properties of zircon are mentioned in Table 2.1 [9]. Though it is the standard value, the actual value differs from the standard due to sources, conditions and presence of impurities. Zircon as an ancient metamorphic mineral, sometimes contains U and Th. A few zircons go through metamictization. Connected to inner radiation harm some modification may observed in zircon. The modification may be decrease of density, colour change, disruption of crystal structure and so on. [12,16].

Table 2.1: Physical Properties of Pure Zircon [9]

Number	Properties	Value
1.	Bulk Density (Uncompact)	2643-2804 kg/m^3
2.	Specific Gravity	4.6-4.71
3.	Mohs Hardness	7-7.5
4.	Melting Point	2100^0 C- 2300^0 C
5.	Co-efficient of linear expansion	7.2 X 10^{-6} cm/cm^{0}C

The diagnostic features of zircon and its physical characteristics like the shape of the crystal colour, hardness, specific gravity etc are different for different sources. Thus it is very important to acquire knowledge on various aspects of its physical properties for better identification.

2.1.3 Applications of Zircon

Zircon and its derivatives have vast range of application as shown in the Fig 2.4. Approximately 54% of zircon is used in ceramic industry which is the largest application of it. 14% goes into foundry,11-14% application is on refractory. Other 19% application is ongoing new applications like glass, 3D printing, implantation, chemical pigment etc [18].
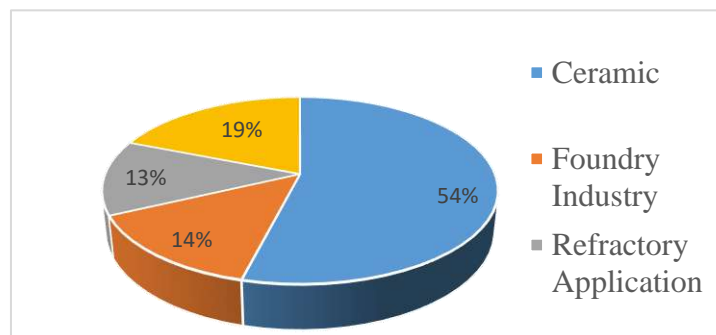
Fig 2.4: Market Condition of zircon and its derivatives [18]

(a)

(b)

(c)

(d)

(e)

Fig 2.5: Application of zircon (a) gemstone (b) opacifier (c) plasma screen (d) refractory brick (e) nozzle of tundish

2.1.4 Zircon Reserve in Bangladesh

In Bangladesh zircon is found as beach sand heavy mineral placer deposits on the sea beaches and coastal islands of Cox's Bazar, Chittagong, Noakhali and Patuakhali districts along with other deposits. The present mineral reserve is about 4.4 million tons as shown in Fig 2.5 [19].
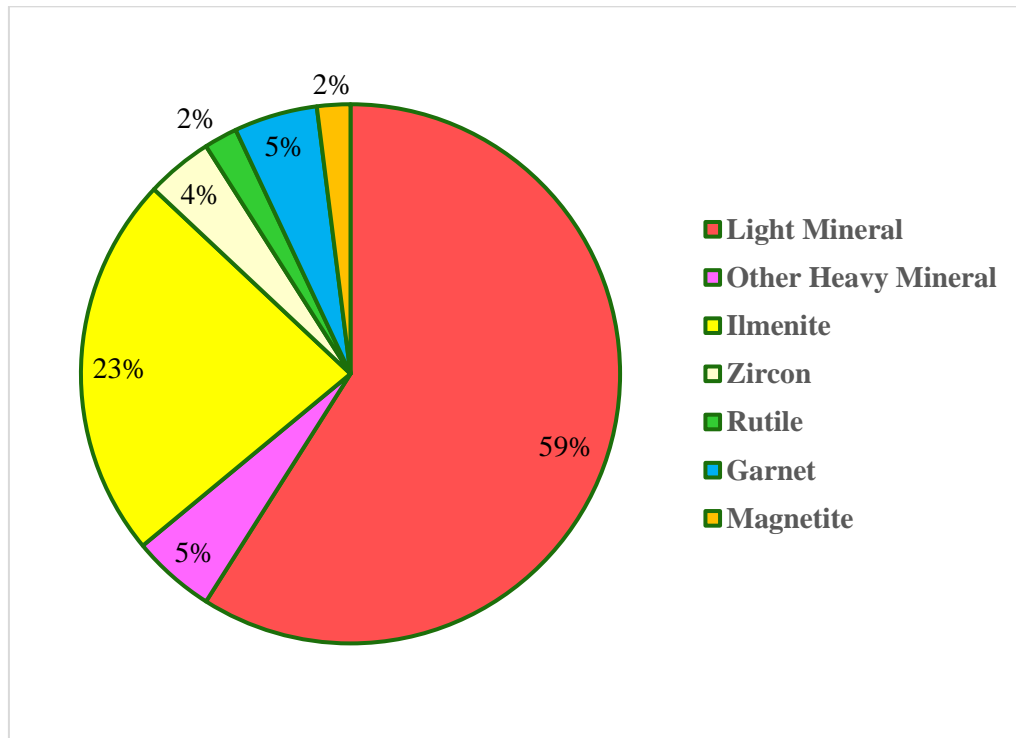
Fig 2.6: Mineral Reserves in Bangladesh [19]

Zircon occurs mostly with fine to very fine sand grains. Generally, the sand containing it are even finer than the sands containing ilmenite, garnet and rutile. The highest concentration of zircon, reported from Shilkhali, is 7%, the lowest concentration is 1% and the average is 4%. The reserve of zircon in Bangladesh is about 158,117 ton [20].

Table 2.2: Reserve of zircon at different localities in Bangladesh [20]

Locality	Raw Sand	Heavy Mineral	Zircon
Badarmokam (Cox's Bazar)	1765000	411000	4932
Sabrang (Cox's Bazar)	347558	68582	4184
Teknaf (Cox's Bazar)	1939580	442291	28306
Shilkhali (Cox's Bazar)	2756828	489714	33300
Inani (Cox's Bazar)	729286	175476	10880
Cox's Bazar	5119000	920000	23000
Maheshkhali Island (Cox's Bazar)	4114230	784210	37112
Matarbari Island (Cox's Bazar)	69030	15215	794
Nijhum Island (Noakhali)	379337	96348	2052
Kutubdia Island (Cox's Bazar)	404646	120000	3900
Kuakata (Patuakhali)	2872486	831668	9647
Total	20496981	4354504	158117

2.2 Overview of Zirconia

Zirconium di oxide or zirconia (ZrO_2) can be found as natural form of mineral baddeleyite. Mostly it is derived from zircon. It is the most commercially important oxide formed by zircon. Zirconia is a crystalline solid which is white in colour, but can be produced in different colours. It is known as **"ceramic steel"** for being chemically inert and is considered as one of the highly auspicious restorative materials, due to its excellent mechanical properties. Out of all advanced ceramic materials, at room temperature zirconia has the highest toughness and strength [21]. At high temperatures, zirconia may go through substantial change in volume during phase transformation [5]. Because of the polymorphic behavior, outstanding mechanical properties, zirconia and zirconia based ceramics are considered as best potential materials within the engineering ceramic field.

2.2.1 Crystal Structure of Zirconia

Zirconia does not occur in nature. At ordinary temperature it has hexagonal closed packed crystal structure and forms number of compounds i.e. zirconate (ZrO_3^{-2}) and zirconyl (ZrO^{+2}) salts. Zirconia is obtained as a white powder and possesses both acidic and basic properties. Zirconium oxide crystals are arranged in crystalline cells (mesh) which can be categorized in three crystallographic phases: cubic (C) in the form of a straight prism with square sides, the tetragonal (T) in the form of a straight prism with rectangular sides and the monoclinic(M) in the form of a prism with parallelepiped sides as shown in Fig. 2.7 [22,23].

0 < T <1170 ºC	1170 < T < 2370 ºC	2370 < T < 2950 ºC
ZrO$_2$(monoclinic), 5.6 g/cm³	ZrO$_2$(tetragonal), 6.1 g/cm³,	ZrO$_2$ (cubic) 6.3 g/cm³
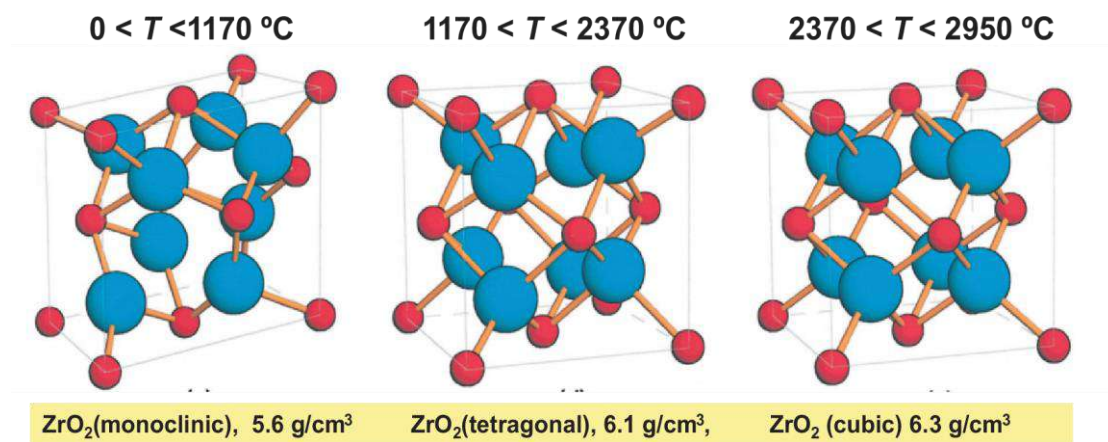
Fig 2.7: Different polymorphs of zirconia [21]

From phase diagram, Fig 2.8 it is found that the monoclinic form is stable at room temperatures and up to 1,170°C. Above this temperature it transforms into the denser tetragonal phase with a volume decrease of 5%. The tetragonal phase is stable between 1,170ºC and 2,370°C and above this temperature it acquires a face centered cubic crystal form. During cooling, a T-M transformation occurs in a temperature range from 670ºC to 1,070°C, followed by a volume expansion of approximately 3 to 4% [23].
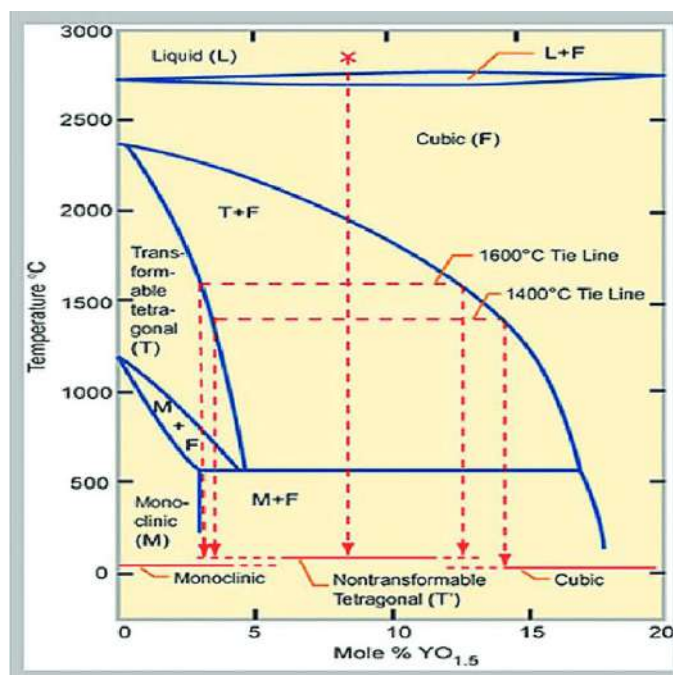
Fig 2.8: Phase diagram of partially stabilized zirconia [23]

This phase transformation generates stresses that result crack formation. In the presence of a small amount of stabilizing oxide additives (eg, CaO, MgO, Y_2O_3), the tetragonal particles provided are small enough and can therefore be maintained in a metastable state at temperatures below the tetragonal to monoclinic transformation temperature. At room temperature, tetragonal metastable zirconia exists only in particles of less than 30 nm. This stability is due to the lower surface energy of the tetragonal phase compared to the monoclinic, or due to the constrain of rigid matrix on the tetragonal grains [24].

2.2.2 Properties of Zirconia

Zirconia has excellent resistance to chemicals and corrosion without the typical brittleness common in technical ceramics. When compared to other advanced ceramic materials, zirconia has exceptional strength at room temperature [24]. Other principal properties of this material include high fracture toughness, high density, high hardness and wear resistance, good frictional behavior, high temperature capability up to 2,400ºC, non-magnetic, low thermal conductivity, electrical insulation, coefficient of thermal expansion

similar to iron, and modulus of elasticity similar to steel. Over the years, a new name was coined for zirconia called 'ceramic steel' [21]. The above mentioned properties are high enough to allow zirconia to be an effective material for many applications, especially for refractory and dentistry purposes [25]. Some of the outstanding mechanical properties of zirconia are appended in table 2.3.

Table 2.3: Properties of zirconia [25]

Mechanical Properties	Value
Density	6.05 g/cm^3
Mohs Hardness	8-8.5
Bend strength	900-1200 MPa
Compressive strength	2000 MPa
Fracture toughness	7-10 MPam$^{\frac{1}{2}}$
Young's modulus	210 GPa
Elastic Modulus	100 – 250 GPa
Thermal expansion coefficient	11x10^{-6} 1/K
Tensile Strength	330 MPa

2.2.2.1 Tribological Property of Zirconia

The demand for decreasing CO_2 emission and harmful material content of exhaust gas of passengers' cars requires improvement of powertrain including the applied lubricants. Zirconia nanoparticle is now using as lubricant additives due to its tribological property. Zirconia has high chemical resistance even strong acid can barely attack ZrO_2. It has strong corrosion- resistance properties without the brittleness like the typical ceramics. Frictional losses are the main sources of waste energy in mechanical system. To reduce frictional losses zirconia doped lubricants are used [26]. Some of the working mechanism of zirconia nanoparticles as lubricants are shown in the Fig. 2.9.
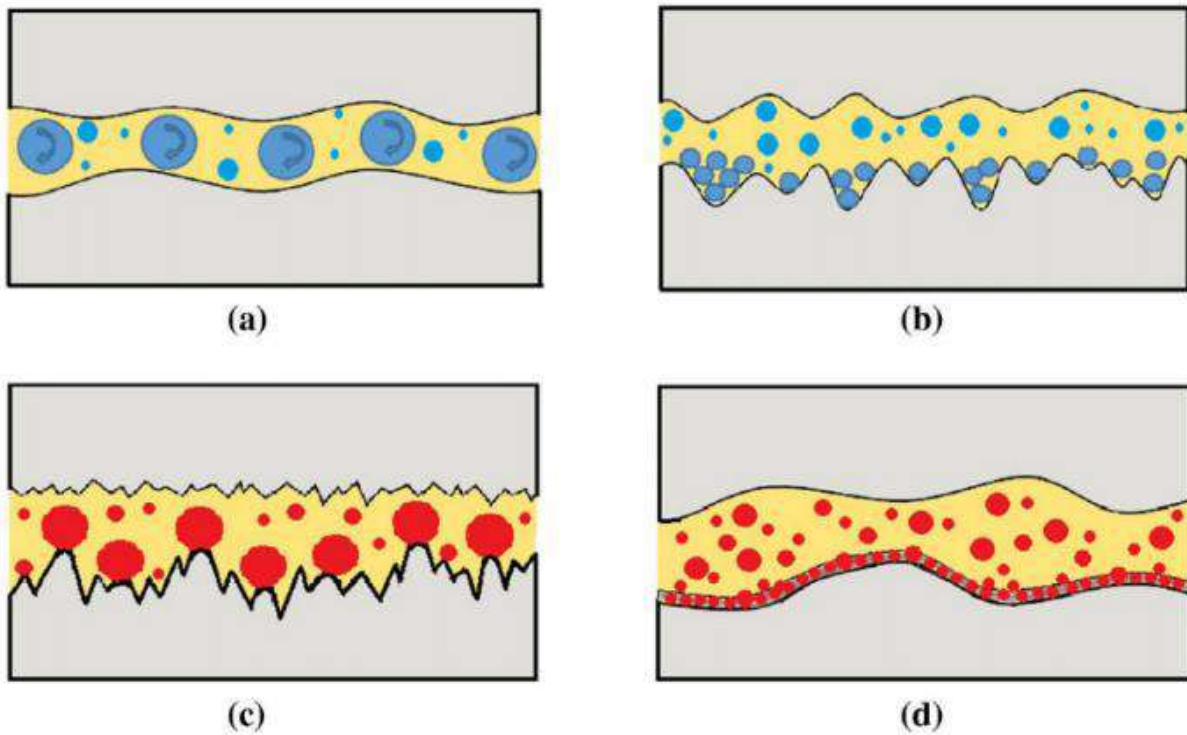
Fig 2.9: Different working mechanisms (a) rolling (b) mending (c) polishing (d) protective film for increasing the tribological performance by using ZrO_2 nanoparticle [27]

2.2.2.2 Thermal Property of Zirconia

Thermal conductivity and thermal expansion of ZrO_2 is very low 1.7 W/m.K and 11×10^{-6}/K. It is the most suitable material for thermal barrier coating (TBC) on gas turbine or other high temperature exposed machine components. Generally, TBC coating is given to Ni base superalloy to protect them from melting, oxidation or thermal fatigue. To be TBC material one must be fulfill the requirements shown in Fig. 2.10. The TBC material must be chemically inert and be heat and oxidative resistant. It should have high melting point and low thermal conductivity to protect Ni based superalloy from high heat and corrosion.
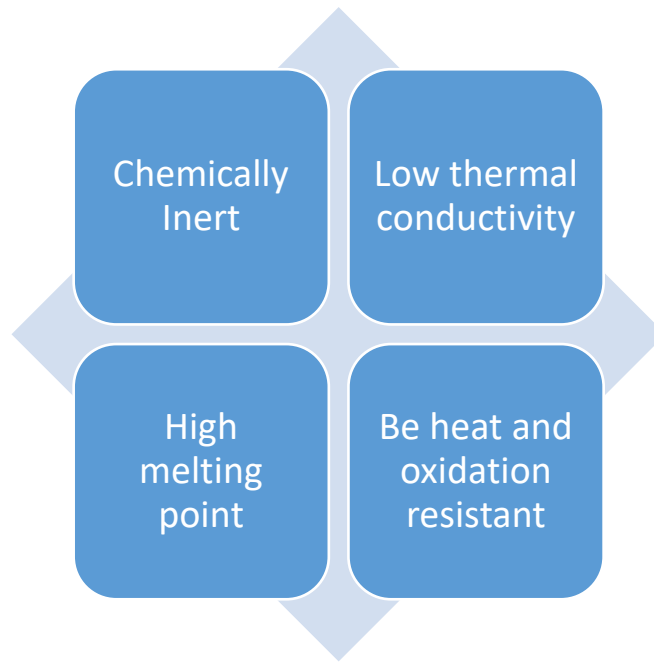
Fig 2.10: Requirements of TBC material

Yttria-stabilized zirconia is used as TBC material as because it is chemically inert, low conductive, possess high melting point, heat and oxidation resistant etc. It creates strong bond with substrate which is called top coat as shown in Fig. 2.11. The ceramic layer creates the largest thermal gradient of the TBC and keeps the lower temperature than the surface. The low and temperature independent thermal conductivity of YSZ was attributed to the presence of a high point defect concentration associated with a substitution of Zr^{+4} ions by Y^{+3} ion in fluorite structure, producing a small spacing between point defects. High concentration of oxygen and ion vacancies made thick thermally grown oxide [28]. In this way, complex chemistry of ZrO_2 protects the base superalloy from heat, oxidation, and corrosion. This can increase the operating temperature of the base superalloy by several hundred degrees. To obtain better properties researches are being continued by using different fabrication techniques.
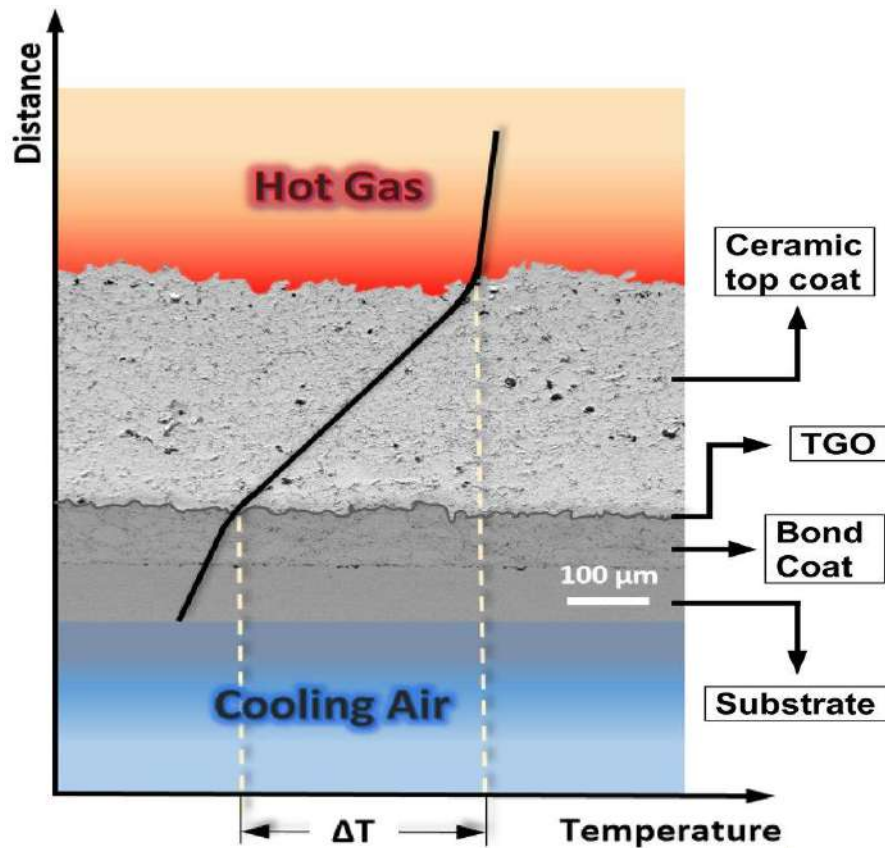
Fig 2.11: Thermal barrier coating system [29]

2.2.2.3 Biocompatibility of Zirconia

Zirconia (ZrO_2) is a bioinert, strong, and tough ceramic. Zirconia ceramics have several advantages over other ceramic materials, due to the transformation toughening mechanisms. As it is operated in their exceptional microstructure, it can show very interesting mechanical property. Transformation toughening is an important indication of clinical biocompatibility [30].

The research on the use of zirconia ceramics as biomaterials started in late sixties and now zirconia (Y-YZP) is in clinical use. Recent developments have concentrated on the chemistry of precursors, in forming and sintering processes, and on surface finish.
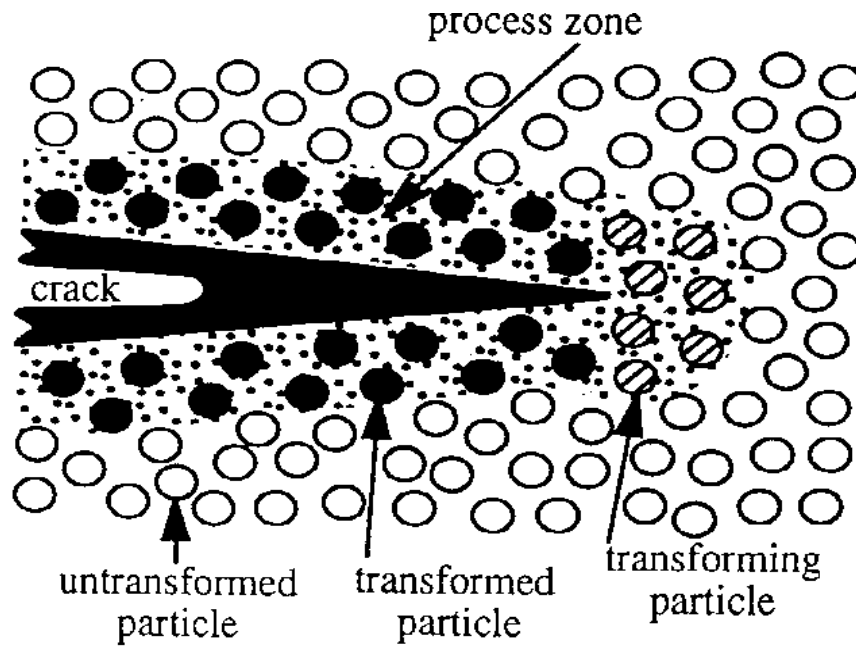
Fig 2.12: A schematic representation of stress-induced transformation toughening process of zirconia [31]

ZrO_2 structure is monoclinic between room temperature to 950°C. More than 950°C ZrO_2 converts to tetragonal which is accompanied by 1% shrinkage on heating and equivalent expansion on cooling. At higher temperature ZrO_2 changes from tetragonal to cubic with proper chemical additions and heat treatment a microstructure can be achieved during cooling that consists of lens shaped precipitation of ZrO_2 tetragonal in cubic ZrO_2 grains. Normally the transformation from tetragonal to monoclinic during cooling tends to expand the structure but high strength of cubic ZrO_2 prevents this expansion. So, tetragonal structure is retained all through the way to room temperature. The same thing happens when the crack tries to form and break the ceramics [30]. Tetragonal precipitates next to the crack are now able to expand and transform back to their stable monoclinic form. This expansion adjacent to the crack presses against the crack and stops it [31]. This is the mechanism named transformation toughening which is the main mechanism of any biocompatible material. The mechanism is shown in Fig. 2.12.

2.2.3 Applications of Zirconia

As zirconia shows many useful properties that allow its' nanoparticle to be suitable for a variety of purposes across many industries. Most common uses of zirconia are production of hard ceramics and refractory materials like refractory bricks and armour plates etc [32]. This material is most widely used for production of various dental and bone implants due to its hardness, chemical un reactivity, and its biocompatible aspects as stated earlier [24]. Some of the common uses of zirconia is shown in Fig 2.13.
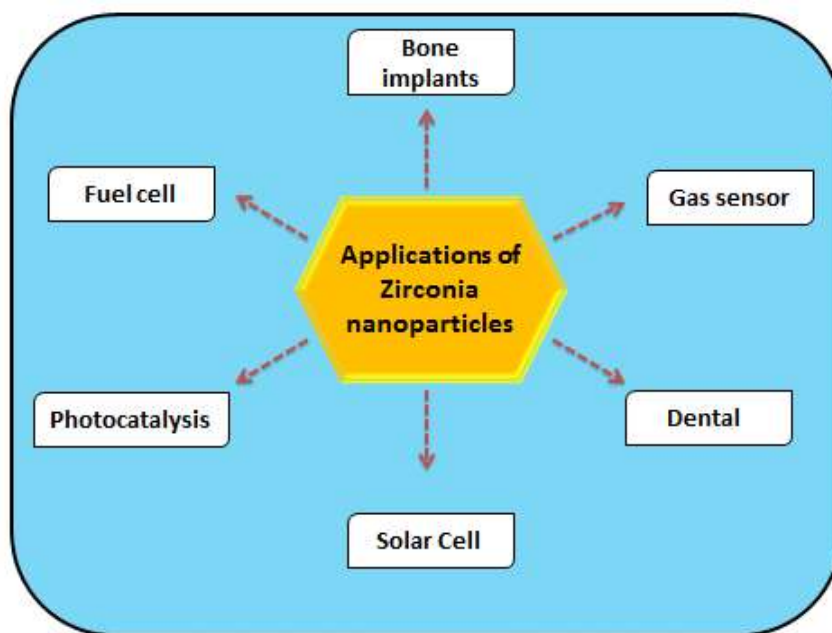
Fig 2.13: Application of zirconia nanoparticles [32]

One of the modern applications of zirconia is solar cell where zirconia film coating is used. Beside it, zirconia is being used in fuel cell membranes and oxygen sensing mechanisms even at elevated temperatures [24]. Moreover, the jewelry value of zirconia can't be neglected as cubic zirconia is a viable alternative of diamond [25]. The photocatalysis behavior of zirconia showed wide range of use in degradation of textile dye. The photocatalysis behavior varies with band gap of crystal structure. The discussion will be elaborated in the subsequent sections. Some of the applications of zirconia-based materials are shown in Fig 2.14.

(a)

(b)

(c)

(d)
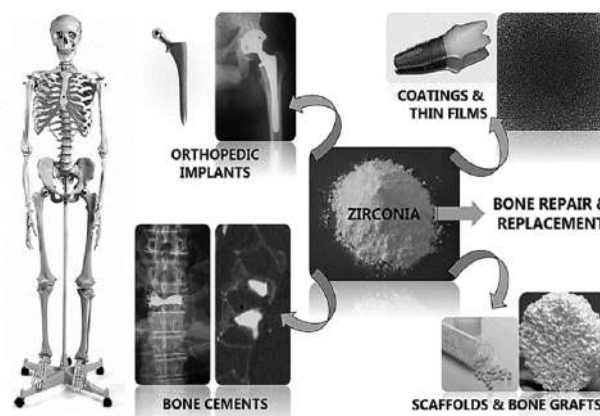
(e)

Fig 2.14: Application of zirconia (a) mortar (b) dental crown (c) jewelry (d) Thermal barrier coating with zirconia in turbine (e) bone implantation

2.3 Demand Situation

The zircon and zircon-based market is expected to witness a healthy growth, at an estimated over 5% in terms of volume, over next five years. The major factors driving the growth of the market studied are the consistent growth in foundries and refractories, growth of nuclear power stations in Asia-Pacific, and the accelerating usage in surface coatings [33]. Global demand situation of zircon is illustrated in Fig 2.15.
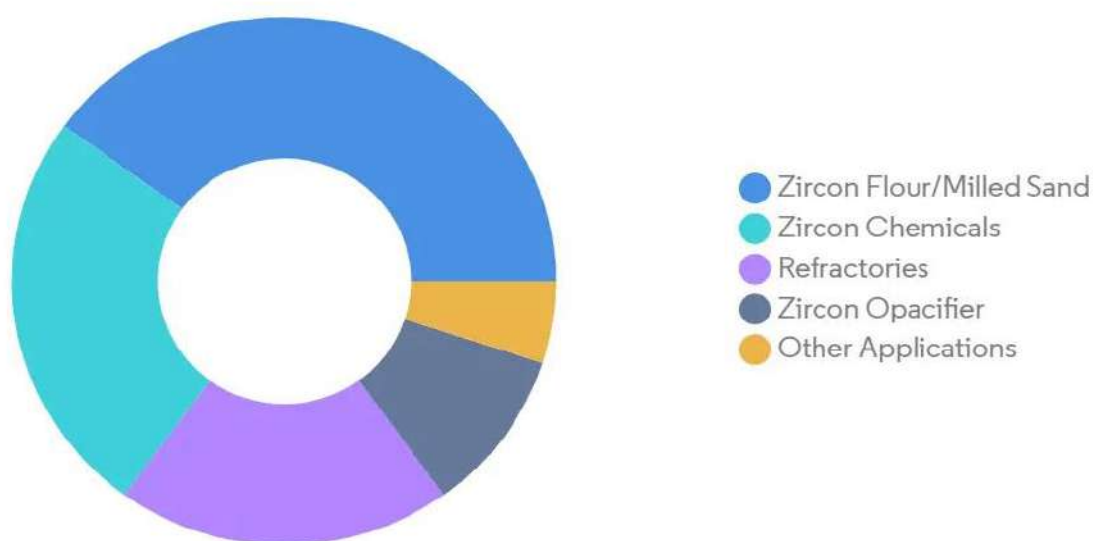
Fig 2.15: Global zircon market, volume share (%) by application (2021) [33]

Reducing dependence on zircon is expected to hinder the growth of the market. Zircon segment accounted for the largest share of about 70% of the total volume of the market. China was found to be dominate the market with about 50% of the total revenue. Still in case of production Australia is expected to dominate the market whereas China would likely to be the main consumer in the world as earlier [33]. Market forecast of zircon and zircon based products are shown in Table 2.4.

Table 2.4: Market forecast of zircon and zircon-based product on basis of volume [33]

	Production	Consumption
Geography of Zircon	Australia	China
	Brazil	US
	China	Japan
	India	EU
	Indonesia	India
	South Africa	Russia
	Ukraine	Spain

2.4   Beneficiation Techniques

Beneficiation of metals deals with extraction of metals from naturally occurring compounds known as ores and their refinement to a purity suitable for commercial use. The extraction of minerals and ores resembles ore-dressing and beneficiation which is dealt with extractive metallurgy. Pyrometallurgy, hydrometallurgy and electrometallurgy are the three sub headings of extractive metallurgy which is one of the main concerns of metallurgist [34].

2.4.1   Pyrometallurgical Processes

Pyrometallurgy generally deals with reduction reaction which requires energy. This process both use for extraction and purification. Cu, Zn, Fe, Cr, Sn, Mn etc are generally extract by pyrometallurgical route.

Energy input is required to sustain the temperature at which the process takes place. As reaction temperature increases the rate of chemical reaction as well as kinetics also increases. The energy is usually provided in the form of combustion or from electrical heat. When sufficient material is present in the feed to sustain the process temperature solely by exothermic reaction (i.e. without the addition of fuel or electrical heat), the process is said to be "autogenous" [35]. A pyrometallurgical process flow chart of Cu extraction is shown in Fig 2.16.
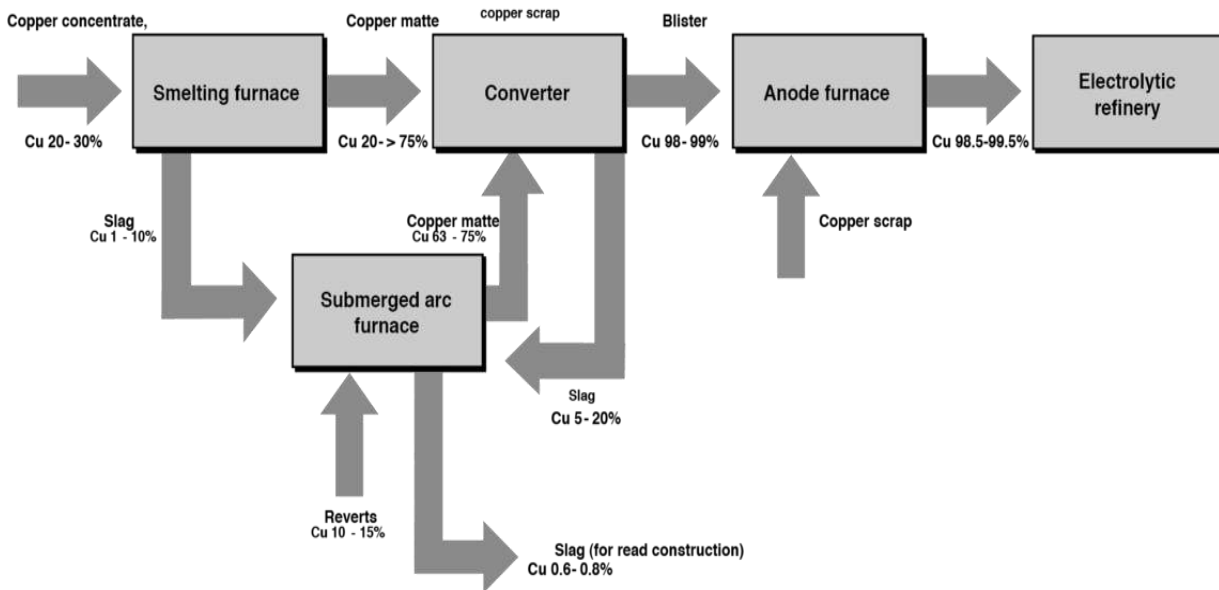
Fig 2.16: Process flow chart of pyrometallurgical process route of Cu [35]

Pyrometallurgical processes are classified as four different processes as specified in Fig. 2.17.
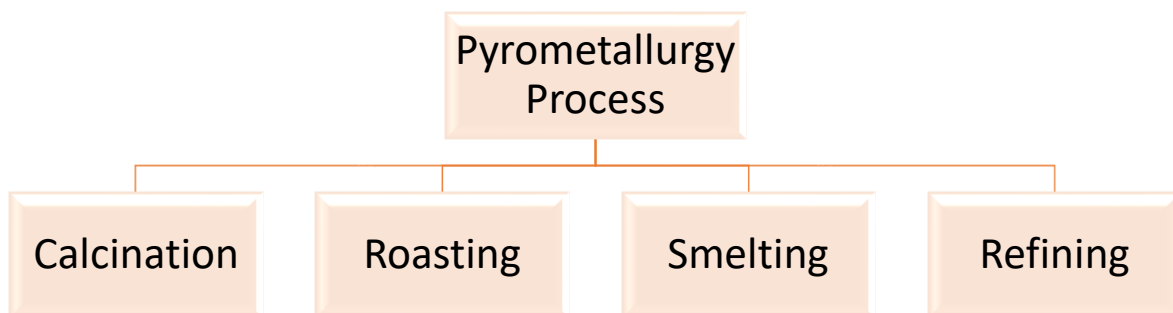
Fig 2.17: Classification of pyrometallurgical process

Calcination is a pyrometallurgical process which requires thermal treatment of an ore that eliminates the volatile products in the form of carbon-di-oxide, water or organic matter. Here the hot gases do not react with ore but provide heat for necessary decomposition [34].

Roasting is heating an ore below the fusion point in excess of air to bring about chemical conversion to a form that is more suitable for subsequent treatment for ultimate extraction of metal. It requires external source of heat or may be autogenous [34].

Smelting involves thermal reactions in which at least one product is a molten phase. It is an operation or combination of operations for the production of a metal or metal reach phase [35].

Refining is the removal of impurities from materials by a thermal process. This covers a wide range of processes, involving different kinds of furnaces or other plants [35].

2.4.2 Electrometallurgical Processes

Electrometallurgy includes all metallurgical processes which utilize electricity and electrical effects. A large number of operations can be considered as electrometallurgical in nature but here discussion restricts to electrolysis namely electrowinning and electrorefining [34]. A schematic view of electrometallurgical process for Na extraction is shown in Fig. 2.18.

The electrolysis cell contains molten sodium chloride (melting point 801 °C), to which calcium chloride has been added to lower the melting point to 600 °C (a colligative effect). The passage of a direct current through the cell causes the sodium ions to migrate to the negatively charged cathode and pick up electrons, reducing the ions to sodium metal. Chloride ions migrate to the positively charged anode, lose electrons, and undergo oxidation to chlorine gas [39]. The overall cell reaction comes from adding the following reactions:

At the cathode: $2\ Na^+ + 2e^- \longrightarrow 2\ Na(l)$

At the anode: $2Cl^- \longrightarrow 2Cl_2(gas) + 2e^-$

Overall change: $2\ Na^+ + 2Cl^- \longrightarrow 2\ Na(l) + 2Cl_2(gas)$
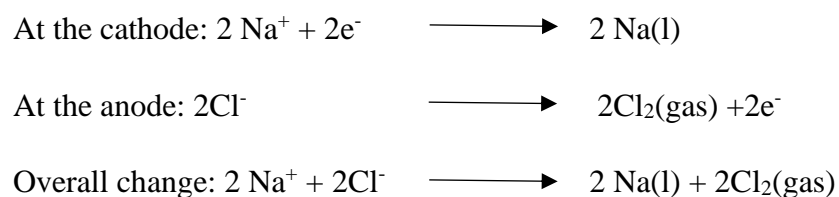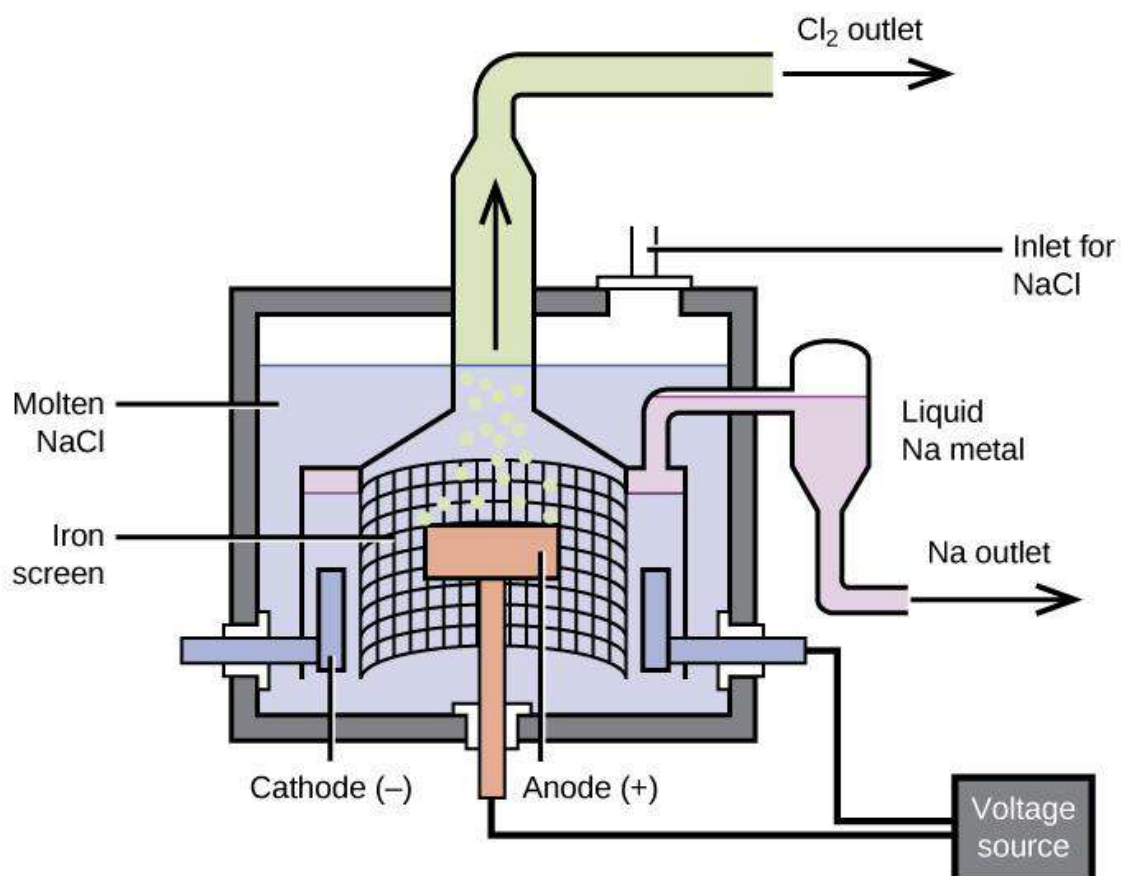
Fig 2.18: Pure Sodium extraction from molten NaCl by electrolysis [36]

In **electrolytic extraction or electrowinning** process the metal is usually in solution in the electrolyte from which it is deposited onto the cathode and the anode is insoluble conductor. It is important for the very reactive light metals like Na, Al, Mg which exclusively produced from fused salt electrolysis.

On the other hand, in **electrorefining** process anode is an impure metal, electrolyte is a solution of electrical conductivity, constant concentration and the cathode is pure metal. High purity Al, Cu is the refined product of electrorefining [34].

2.4.3 Hydrometallurgical Processes

Hydrometallurgy refers to the production of metals or pure compounds with the help of reactions in aqueous solutions especially organic reagents. It is a process of beneficiation as well as extraction. It involves recovery of metals from ores, concentrates, and recycled or residual materials [34]. Hydrometallurgical processes are advantageous over other extractive method due to various reasons like:

- It is suited for lean and complex ores with better control.

- This method is preferable from environmental point of view.

- In context of energy consumption hydrometallurgical method consume less or almost no energy.

- Different physical forms like powder, nodular, coherent surface deposit etc can be recovered by hydrometallurgical route.

- The shortcoming of pyrometallurgical routes can be overcome by hydrometallurgical method like reactive metal extraction, more corrosive metal at temperature etc.

Drawbacks of hydrometallurgical processes is negligible. Generally, this process is not acceptable in mass production due to its lower efficiency. Often it creates significant quantities of waste effluent and tailing product which may be highly acidic or basic.

Hydrometallurgical approaches primarily consist of four process stages: (a) Leaching (b) Separation of leach Liquor (c) Recovery of metallic values (d) Reagent recovery [37]. A general hydrothermal process flow diagram is shown in Fig. 2.19.
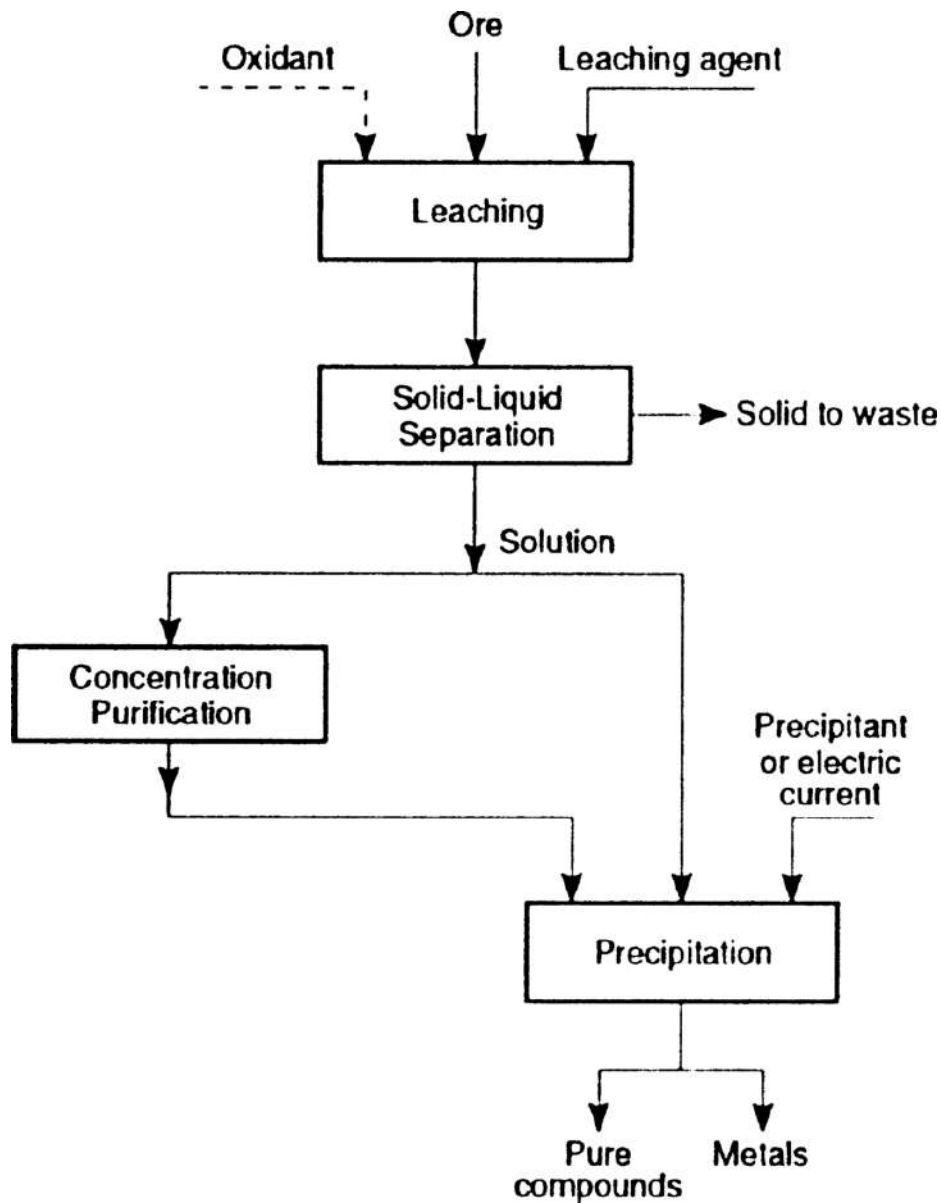
Fig 2.19: A General outline of hydrometallurgical process [37]

Pretreatments before leaching may involve physical or chemical processes to optimize recovery of metals. The pretreatments are as follows.

- ✓ Communication and Concentration
- ✓ Chemical changes in minerals
- ✓ Structure modification.

Leaching involves selectively dissolved the ore in an appropriate solvent which is called leachant. Water, acids, several bases or aqueous salt solutions can be used as leachant. Separation of leach liquor is separation of solid residue from leach liquor. the processes may be settling, thickening, filtration or washing. Evaporation, distillation, ion-exchange precipitation, cementation solvent extraction may employ to enrich the liquor with metal. The leaching agent, is generally recycled after purification and readjustment of composition [34].

2.5   Nanotechnology

Nanotechnology or nanotech, is the use of matter on an atomic, molecular, and supramolecular scale for industrial purposes. It is the manipulation of matter on a near-atomic scale to produce new structures, materials and devices. Nanotechnology comprises with nanomaterials have a length scale between 1 and 100 nanometers [38]. At nano size, materials begin to exhibit unique properties that affect physical, chemical, and biological behavior. Researching, developing, and utilizing these properties is now at the heart of new technology. Though it is unknown about the health-related toxicity of nanotechnology related particles research is continuing to understand how these unique properties may lead to specific health effects [39].

2.5.1   Nanoparticles

Nanoparticles (NPs) are wide class of materials that include particulate substances, which have one dimension less than 100 nm (Laurent et al., 2010). This can refer to a volume, a weight or a unit of time, whereby a nanometer (nm = 10^{-9} meters) corresponds to one billionth of 1 meter. Nanomaterials are up to 10 000 times smaller than the width of a human hair [40]. And this tiny size makes them very valuable for all kinds of practical uses. Depending on the overall shape these materials can be 0D, 1D, 2D or 3D (Tiwari et al., 2012) [41]. Classifications of different nanoscale dimensions are illustrated in Fig 2.20.
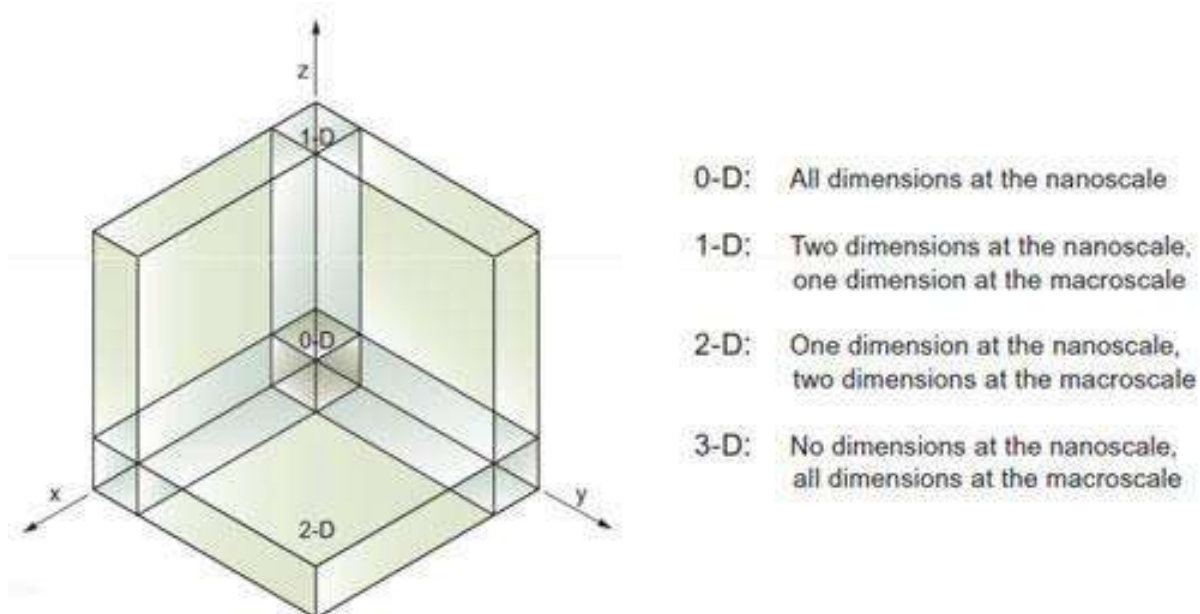
Fig 2.20: Classification of nanoscale dimensions [33]

2.5.2 Properties of Nanoparticles

Materials behave differently at the nanoscale as relative surface area increase and quantum size effect are two principal factors which cause the properties of materials in nanoparticle size to differ significantly from their bulk form [40]. These factors can change or enhance properties such as reactivity, strength and electrical characteristics and so on [41].

Reactivity increase. As a particle decreases in size, a greater proportion of atoms are found at the surface compared to those inside. Almost all of the atoms are on the surface. The surface atoms, as opposed to those inside the material, have fewer direct neighbors and therefore contain so-called unsaturated bonds. These are responsible for the higher reactivity of the particle surface [40].

Quantum size Effect. It describes the physics of electron properties in solids with great reductions in particle size. This effect does not come into play by going from macro to micro dimensions but becomes dominant when the nanometer size range is reached. Nano size particle affect the optical, electrical and magnetic behavior of materials due to quantum size effect [40]. Materials reduced to the nanoscale can suddenly show very different properties compared to what they show on a macroscale. For instance, opaque substances become transparent (copper); inert materials become catalysts (platinum); stable materials

30

turn combustible (aluminum); solids turn into liquids at room temperature (gold); insulators become conductors (silicon) [41].

2.5.3 Synthesis of Nanoparticle

There are two broad approaches to synthesis nanoparticle top down and bottom up. The term 'top-down' approach refers to the mechanical crushing of source material using a milling process. In the 'bottom-up' approach structures are built up by chemical processes . The selection of the respective process depends on the chemical composition and the desired features specified for the nanoparticles [42]. Particle size, chemical composition, crystallinity and shape can be controlled by temperature, pH-value, concentration, chemical composition, surface modifications and process control. Fig 2.21 shows the general mechanism of top-down and bottom -up approach.
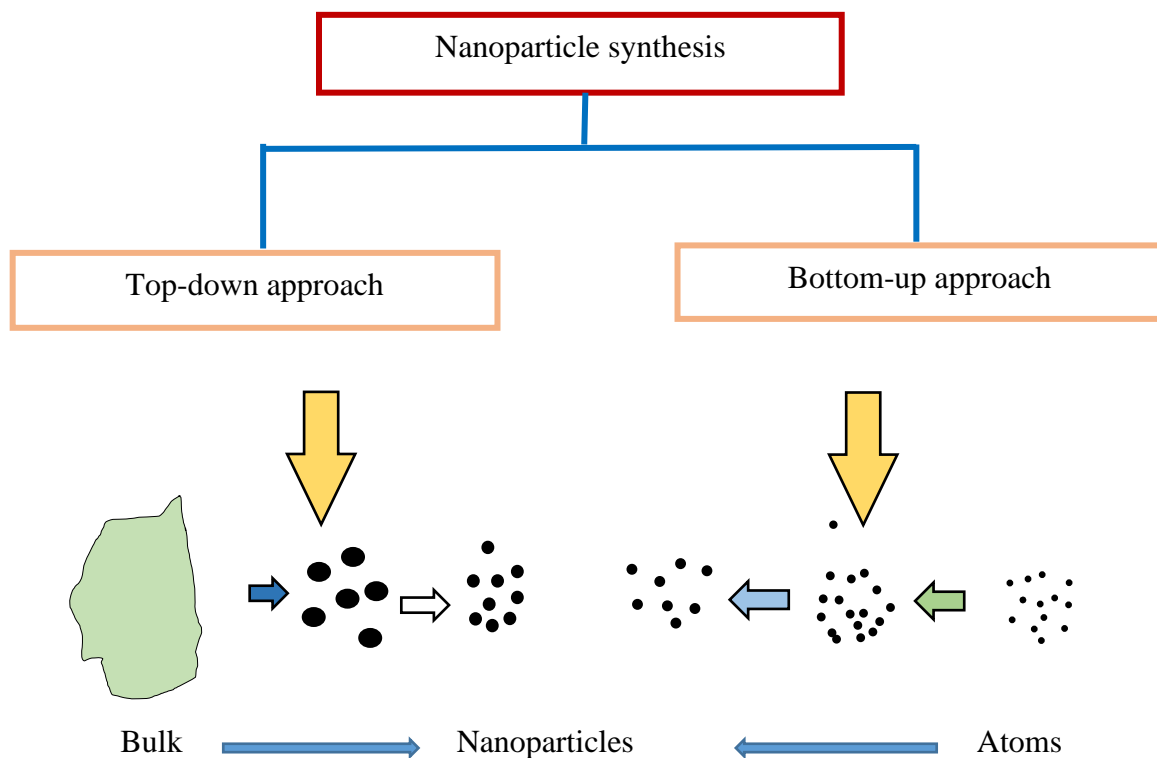
Fig 2.21: Approaches of nanoparticle Synthesis: top-down and bottom-up [42]

Top-down approach resembles with physical method and bottom-up approach refers to physical and chemical method. The top-down approach means reduce the size of the structure toward the nanoscale as so material is wasted in some scale. While the bottom-up approach is the formation of large nanostructure from smaller atoms and molecule which produce almost no loss of product. Some of the methods under broad categories of top-down and bottom- up approaches of nanomaterial synthesis are shown in Table 2.5 [43].

Table 2.5: Methods of nanoparticle synthesis

	Top-down Approach	**Bottom-Up Approach**
Methods of Nanoparticle Synthesis	Mechanical (Ball Milling)	Condensation
	Chemical Technique	Sol-gel
	Thermal (Laser Beam)	Chemical Vapor Deposition
	Explosion Process	Spray Pyrolysis
	Lithography	Hydrothermal

Each of the method has its limitations and fine production capacity of nanoparticles. The top-down approach is quite a feasible technique resulting in the production of a large mass. Mechanical milling or ball milling is most commonly used top-down method for nanoscale synthesis. But the disadvantages associated with top-down are surface imperfections and in some case particle may get damaged [42].

The bottom-up approach by coalescence or assembling of atoms by atoms, molecules by molecules, cluster by cluster to generate a diverse range nanoparticle. It is complex and time-consuming method. Condensation, sol-gel, chemical vapor deposition, spray pyrolysis, hydrothermal etc are some of the bottom-up techniques which are widely used. Henceforth, bottom-up is an amenable technique for creating nanoclusters intended for various applications [43]

2.6 Synthesis of Zirconia

Zirconia nanoparticle can be synthesized by various techniques from zircon sand as stated in Fig 2.22.
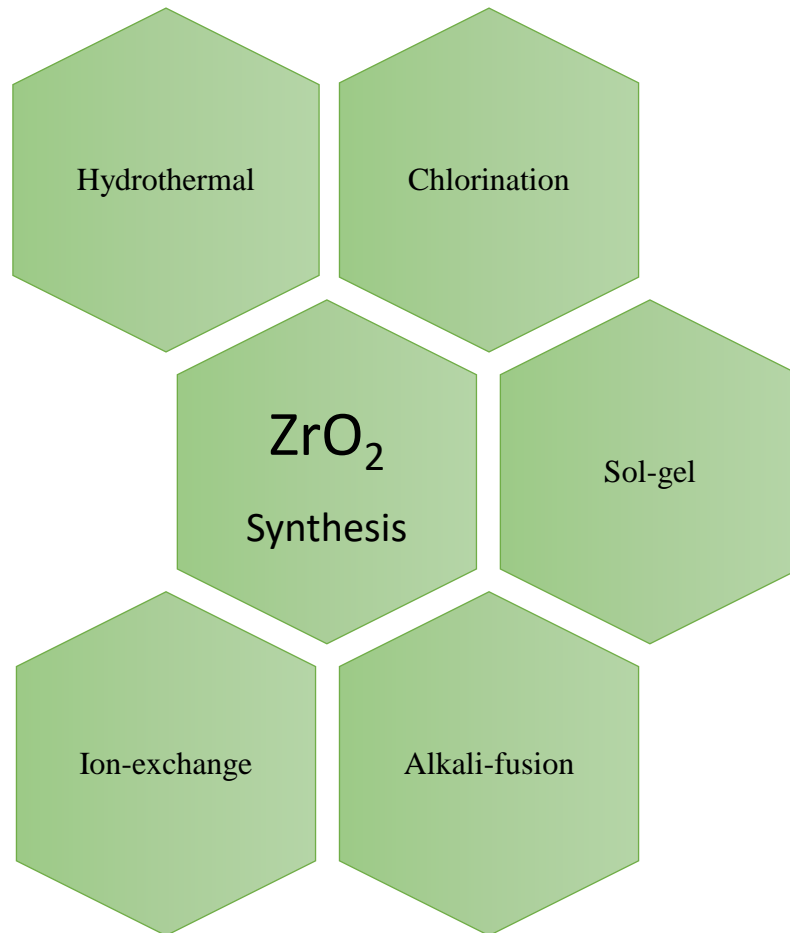
Fig 2.22: Zirconia synthesis techniques

2.6.1 Hydrothermal Decomposition

A hydrothermal process in nature involves the formation of new minerals under the action of water at high temperatures and under high pressures. Hydrothermal decomposition is traditionally used to produce pure and alloyed zirconia from zirconium. Researchers currently show interest in hydrolysis in acid medium, which may be related to hydrothermal decomposition. The starting materials in this process are water solutions of zirconium acetate $ZrO(CH_3COO)_2$, zirconium oxynitrate $ZrO(NO_3)_2 \cdot 2H_2O$, and

zirconium oxychloride $ZrOCl_2 \cdot 8H_2O$ in acid medium (pH 1–2) [45]. A schematic view of zirconia synthesis by hydrothermal process is shown in Fig 2.23.
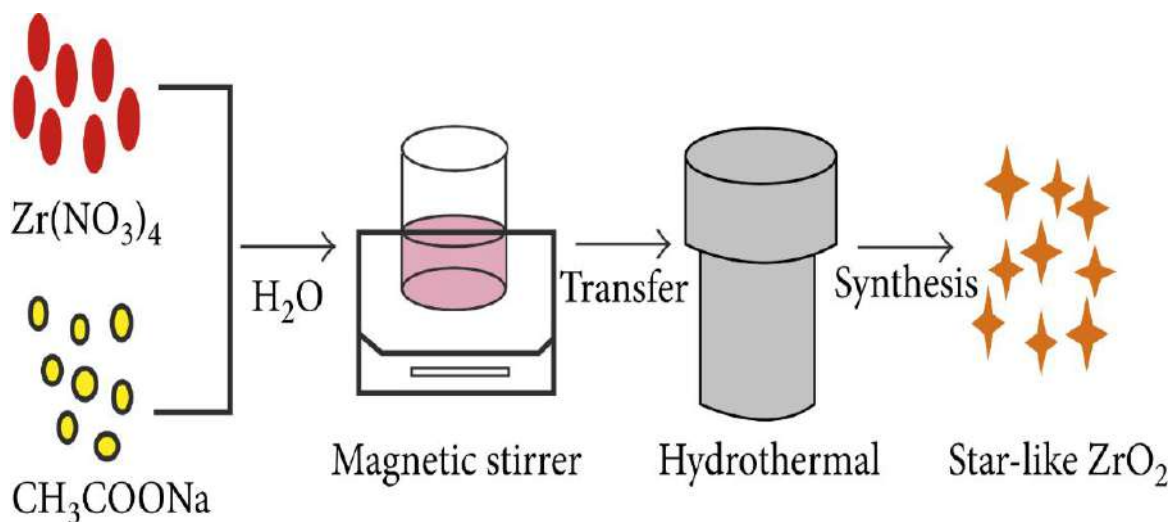
Fig 2.23: Zirconia synthesis by hydrothermal process [44]

2.6.2 Chlorination

The chlorinated zircon which consists mainly of zirconium tetrachloride and silicon tetrachloride are collected and $ZrCl_4$ is calcined at 900°C for 1 hour to produce commercial grade of ZrO_2 [46].

$$ZrSiO_4 + 4\ Cl_2 + 4\ C \rightarrow ZrCl_4 + SiCl_4 + 4\ CO$$
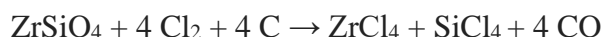
$ZrCl_4$ is also produced by dissolving the zirconium tetrachloride in water, forming the zirconyl chloride which crystallize in the form of $ZrOCl_2.8H_2O$, by either evaporation of the solution or by increasing the acidity by additions of hot hydrochloric acid. The produced zirconyl chloride is calcined at 900°C for 1 hr which yield 99.8% purity of zirconia [46]. A diagrammatic flow chart of zirconia production is shown in Fig 2.24.
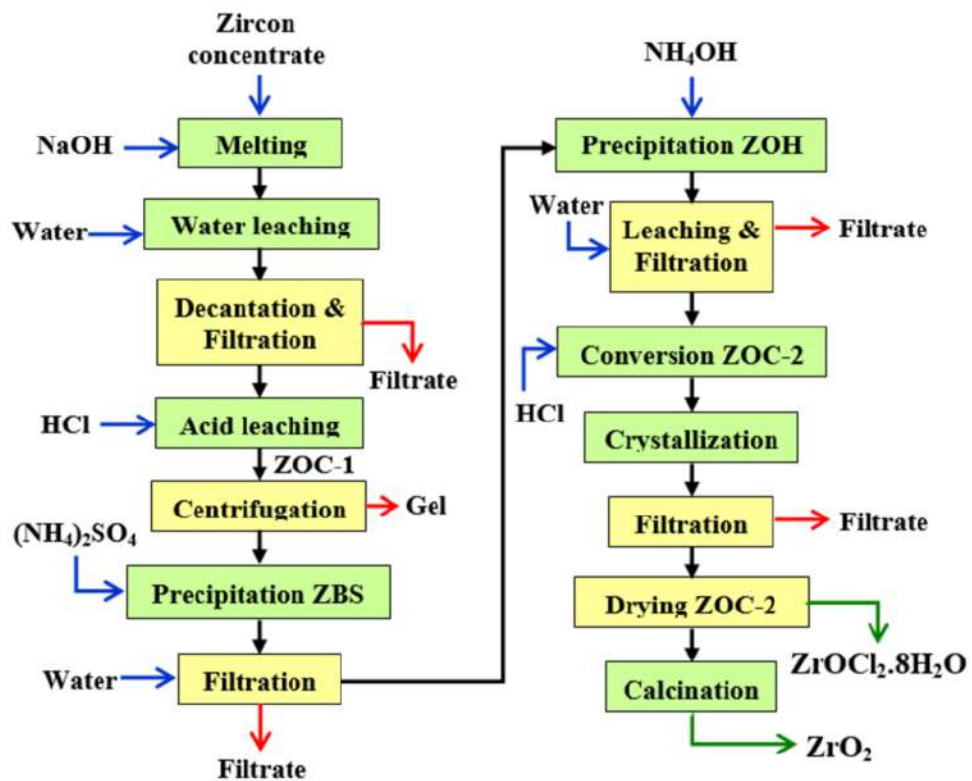
Fig 2.24: The zircon concentrate processing flow chart becomes $ZrOCl_2.8H_2O$ and ZrO_2 [47]

2.6.3 Sol-Gel

Sol-gel technique to synthesize zirconia nanoparticle is a popular one. Zirconium hydroxide can be obtained by the hydrolysis of both zirconium propoxide and zirconium oxychloride precursors. Thermal drying of zirconium hydroxide gel can produce zirconia phase. Depending on the temperature and pressure different phases of crystal structure with different crystalline size can be obtained [48]. A general flowchart of zirconia production by sol-gel technique is shown in Fig. 2.25.
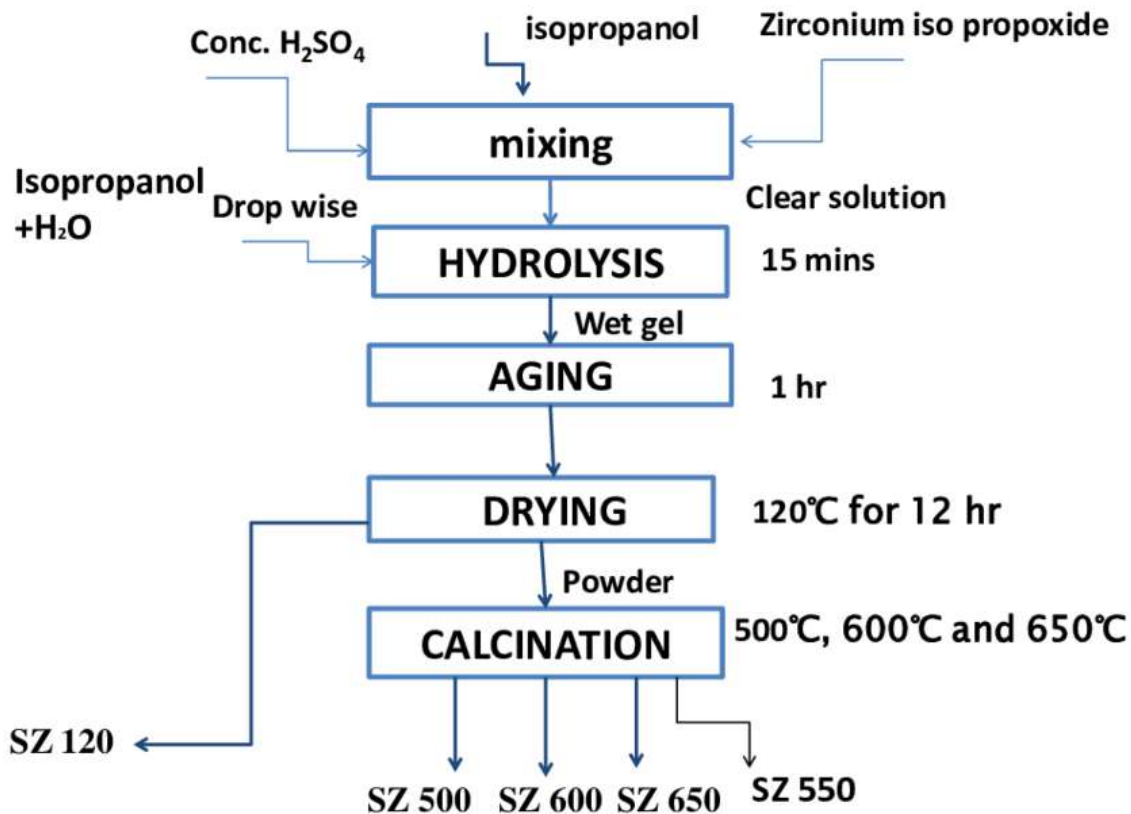
Fig 2.25: A processing flow chart of ZrO_2 synthesis by sol-gel method [49]

2.6.4 Ion-Exchange

The zirconium wet cake (residue obtained after water-leaching alkali-fused zircon) is digested with concentrated acid. The obtained slurry is sufficiently aged and filtered, and the residue is leached with concentrated acid mixture. The slurry is further aged and finally filtered using a filter-aided substrate. The filtrate is passed through an ion-exchange resin. The effluent is treated with 25% (v/v) concentrated sulfuric acid and the resulting zirconium sulfate tetrahydrate is filtered, washed, dried, and calcined at 1000°C for 6–8 hours. A high-purity zirconium dioxide is obtained which has a variety of industrial and scientific applications, especially for the preparation of artificial gems [50].

2.6.5 Alkali-fusion

Alkali-fusion is a well-known process of synthesize zirconia particle from zircon sand. Purity of zirconia yield depends on molar concentration variation of alkali soda. High temperature is used to produce caustic frit with the combination of zircon and alkali soda. To obtain zirconia different methods after alkali fusion has to be employed. The methods are co-precipitation, leaching etc. Fig 2.26 is showing a process flow chart of zirconia synthesis followed by alkali-fusion and leaching.
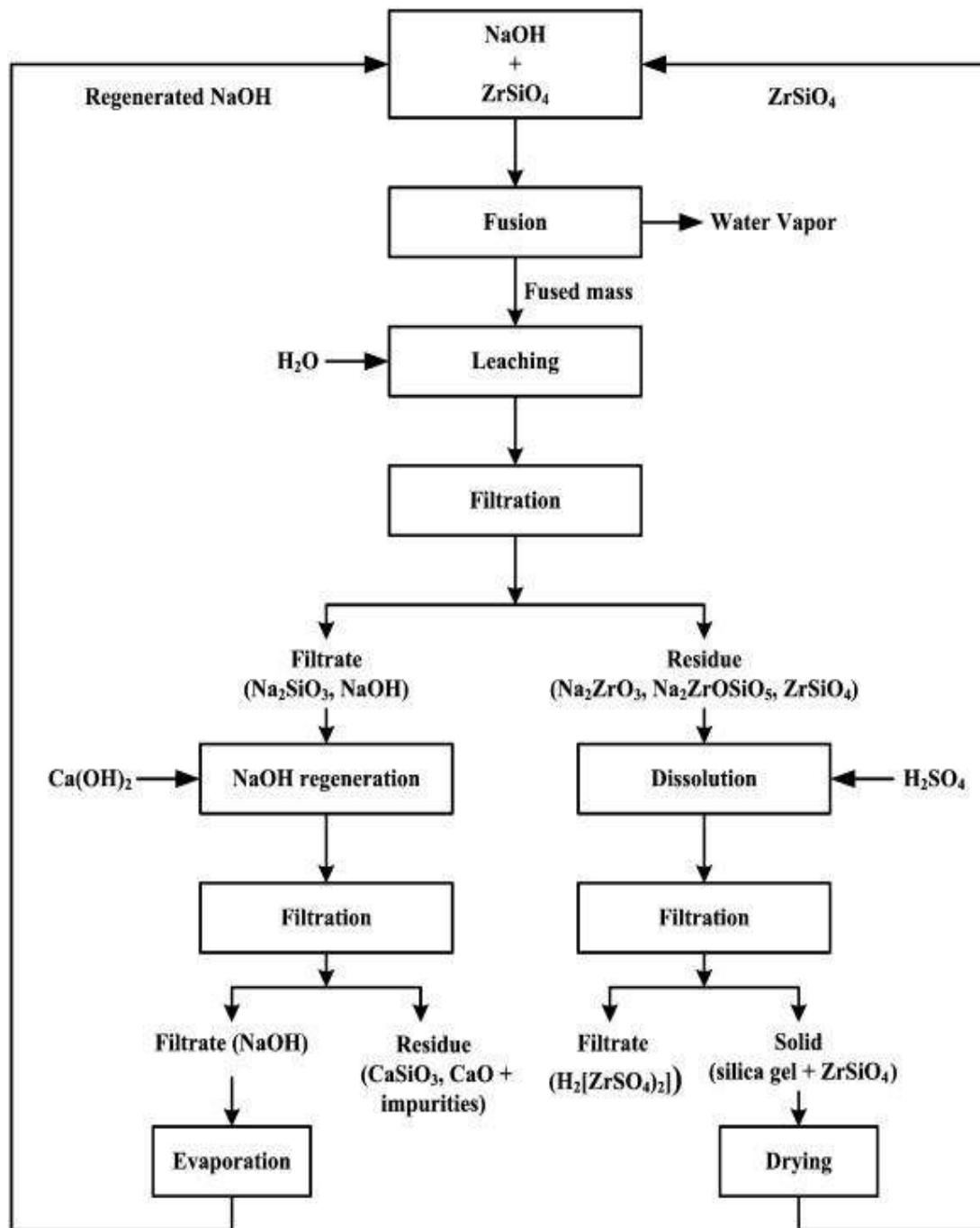
Fig 2.26: A processing flow chart of ZrO_2 synthesis by alkali-fusion method [51]

2.7 Photocatalysis

Effluents from textile dye industries without proper treatment contains remarkable amount of synthetic dyes which are detrimental to environment. It is a big challenge globally to degrade it with eco-friendly way as conventional methods are extremely energy consuming, toxic sludge producer and ineffective [52]. Photo assisted catalysis over a solid semiconductor has been recognized as a promising approach for the removal of organic pollutants such as azo dyes and phenol derivatives. Photocatalysis is used to describe a chemical reaction caused by absorption of ultraviolet (wavelength from 100 to 400 nm), visible light (400 – 750 nm) or infrared radiation (750 – 2500 nm) [53]. A catalyst does not change in itself or being consumed in the overall chemical reaction. This definition includes photosensitization, a process by which a photochemical alteration occurs in one molecular entity as a result of initial absorption of radiation by another molecular entity [53].

2.7.1 Photocatalytic Remedies of Environmental Pollutants

Globally, environmental pollution problems have been increasing day by day since the industrial effluents such as organic pollutants, dyes, heavy metals and radioactive ions were discarded in the rivers, lakes and portable water. The toxicity of these pollutants causes illness to aquatic organisms as well as human health [52]. These toxins are non-biodegradable. Some of the toxins are shown in Fig. 2.27. They would accumulate in the food chain and affect our health. Photocatalytic remedies are promising one as many as different advantages. The advantages are: requiring a simple reactor, no secondary pollution left by the degraded organic substances, and able to be reprocessed in an ecofriendly approach [56].
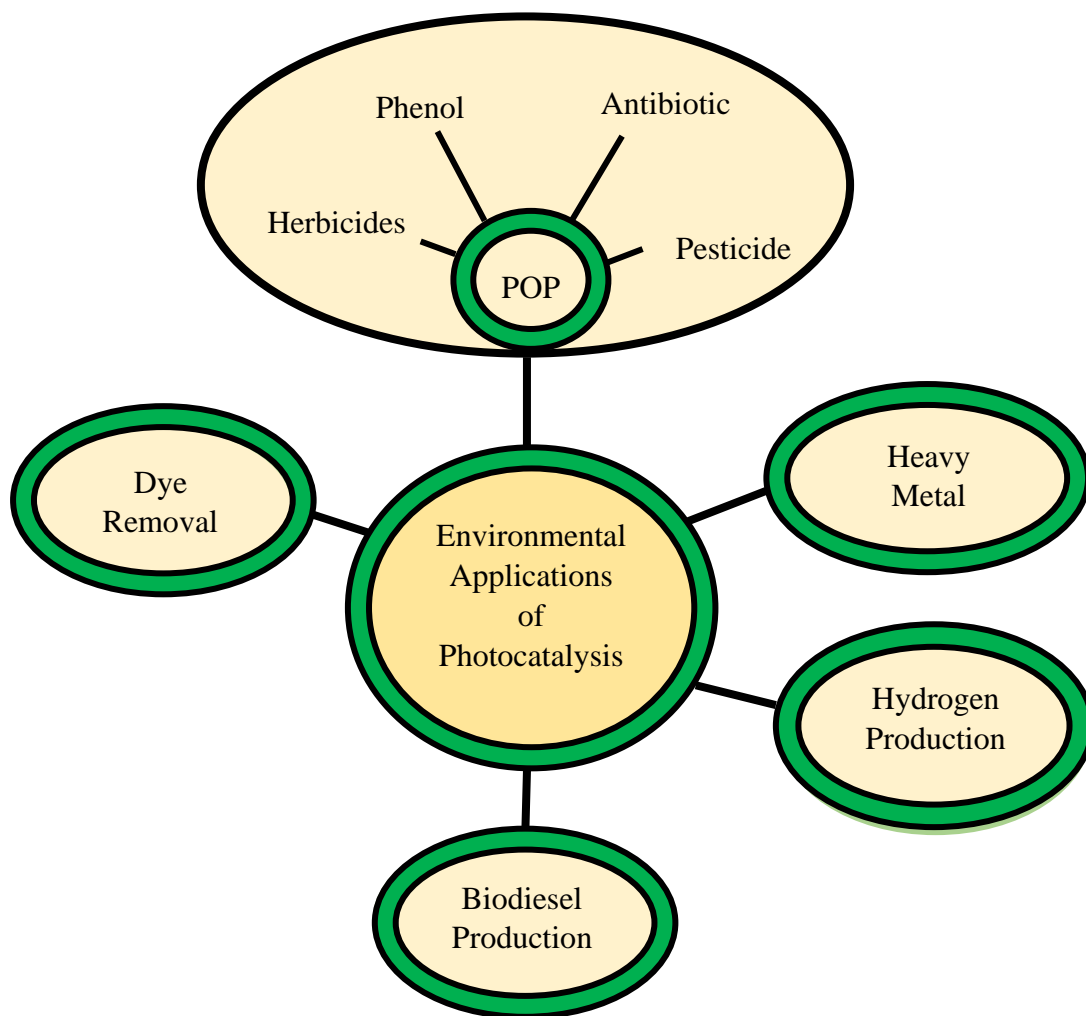
Fig 2.27: Environmental application of photocatalysis process [56]

2.7.2 The Mechanism

Only semiconductor can act as photocatalyst because electronic structure of a semiconductor is characterized by an energy gap between valence band (populated with electron) and conduction band (empty state). Valence electrons can be promoted to the conduction band upon excitation with photons with an energy which is more than band gap energy as shown in Fig 2.28. On the other side, no band gap exists between valence and conduction band in case of metal and large band gap >4eV prevails in case of insulator [54].
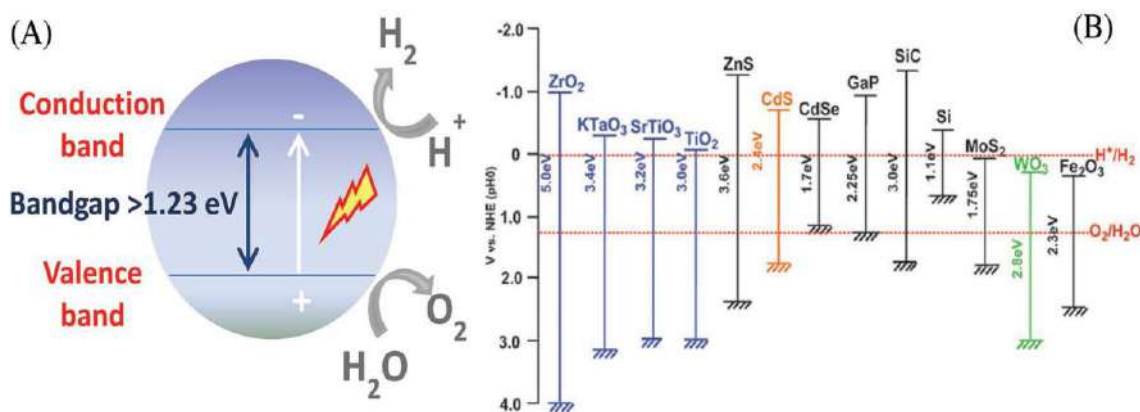
Fig 2.28: Photocatalytic water splitting. A) Schematic of water splitting using semiconductor photocatalyst. B) Band structure of semiconductors and redox potentials of water splitting [55]

Photocatalyst is designed to facilitate reactions of the excited electrons with oxidants to produce reduced products, and/or reactions of the generated holes with reductants to produce oxidized products. The semiconductor photocatalyst on irradiation to light produce holes in valence band and electrons in conduction band which are oxidative and reductive entity. Consequently, these photogenerated charge carriers then react with water or dissolved oxygen to produce $OH^{.}$ and O_2 that decompose pollutants into smaller molecules or inactive micro-organisms [54].

$$\text{Photocatalyst} + h\nu \rightarrow e^-_{CB} + h^+_{VB}$$

$$H_2O \rightarrow \cdot OH + H^{+h+VB}$$

$$\cdot OH + H_2O \rightarrow O_2 + 3H^+$$

$$O_2 + e^- \rightarrow O^-_{2(aq)}$$

$$O_2 + e^- + H_2O \rightarrow \cdot OH_{(aq)} + HO_{2(aq)}$$

$$\cdot OH + \text{dye} \rightarrow \text{Degradation product}$$
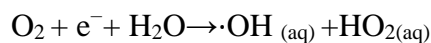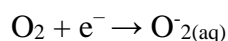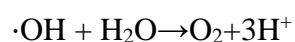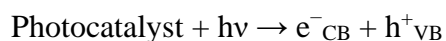
Chapter Three

Experimental

3.1 Sample Collection

For this thesis work sample was collected from sea beach of Cox's Bazar. The initial beneficiation was carried out (Flow Chart 3.1) by Beach Sand Minerals Exploitation Center (BSMEC). Final product was heavy zircon.

Different study on beach sand of Bangladesh has already been performed by BSMEC, Bangladesh Atomic Energy Commission for about decades. The work on zircon from beach sand of Cox's Bazar had also been carried out by different authors [57]. However, the photocatalytic behavior of zirconia, derived from local zircon sand has not been studied yet.
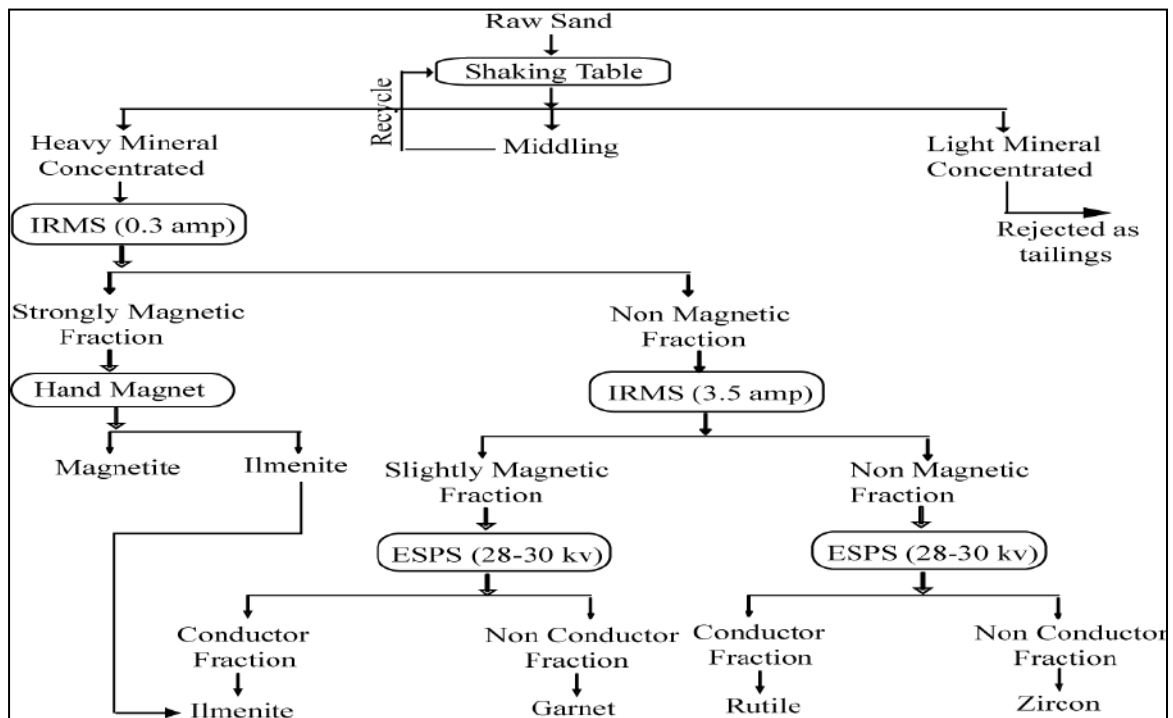
Fig 3.1: Flow chart of zircon extraction from raw sand

3.2 Characterization

The uses of zircon sand depend on its minerology, chemistry, and physical properties. Characterization of zircon plays a vital role in further beneficiary techniques. In this work characterization was performed based on various parameters including morphology, surface analysis, composition, size, density, transportation, moisture content, crystallinity etc. The experiments conducted were totally influenced by locally available facilities.

3.2.1 Material Composition

The characterization begins with bulk chemical analysis of zircon. The results serve as a reference point assessment procedure. The most appropriate technique for detection of major chemical impurities is X-ray fluorescence (XRF). It is non-destructive, multi-elemental, fast and economical if compare to other competitive techniques.

In the present study, XRF was used to determine the chemical composition of the material (Model: Lab Center XRF-1800). The sample for X-ray fluorescence analysis was prepared in the following way:

1) About 2 gm of samples was finely ground in an agate mortar. The prepared powder was made moisture free.
2) The powder was placed in a die and then pressed in a hand press machine to prepare disk shaped sample for analysis.
3) The disk shaped samples were placed in the machine for analysis.
4) During analysis the following operating condition were maintained:

      Atmosphere: Vacuum; Spin: On

      Channel: Radiation- 40 KV;95 mA; For Oxide- 20 deg /min; Step :0.10

      P10 gas (90% argon and 10% methane gas mixture) flow rate: 5ml/min
      Water flow rate: 4.1 L/min.

3.2.2 Morphology

The colour, size and shape of the samples were studied under stereo microscope first (Model: Stereo Microscope-Japan). To understand the morphology samples were observed

via polarizing microscope (Model: LEICA-ICC50E-Germany) with the help of Michel-Levy interference colour chart.

Michel-Levy chart:

Quantitative analysis of the interference colours observed in birefringent samples is usually accomplished by consulting a Michel-Levy chart. From the traditional Michel-Levy chart [58,59], it is evident that, the polarization colours visualized in the microscope and recorded onto film or captured digitally can be correlated with the actual retardation value, thickness, and birefringence of the specimen. In short, it is a key to identify minerals. Most optical microscopes are equipped with ¼-lambda and 1-lambda plates and hence one can rely on different versions of the Michel-Levy interference colour charts. This is commonly a big challenge not helped by the mismatch between observed interference colours and those displayed in the charts. That is why further studies are done to revise the chart.
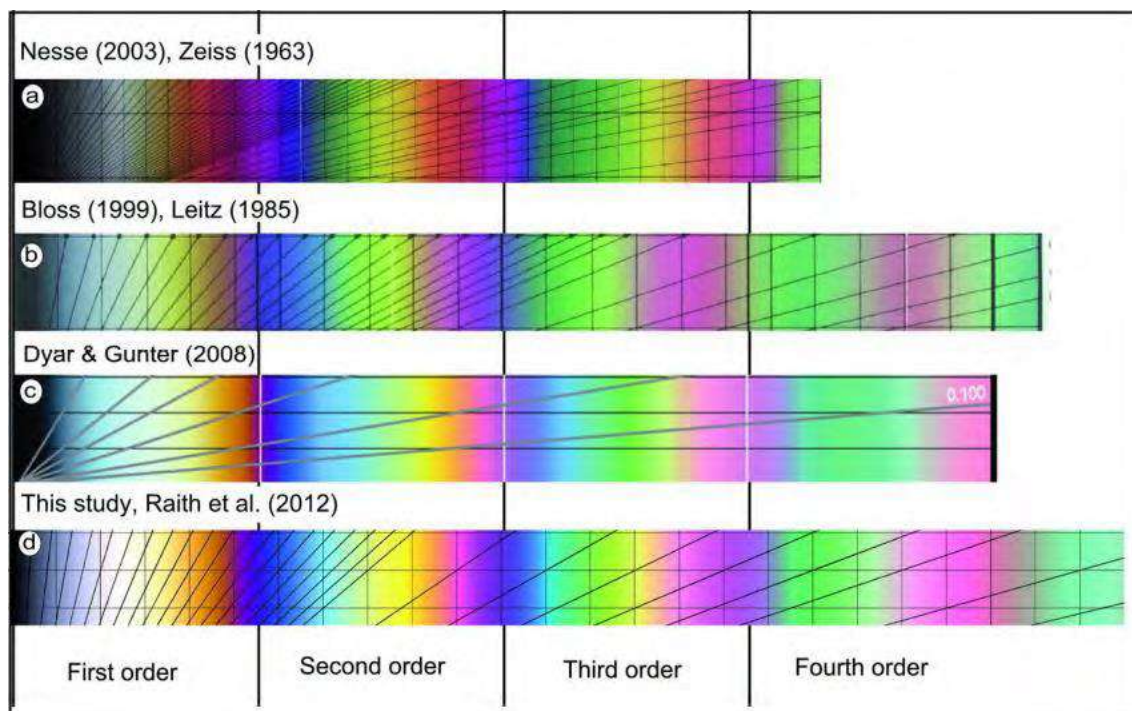
Fig 3.2: Comparison of the new chart with other available and commonly used charts. (a) The Zeiss chart, also used in Nesse (2003). (b) The Leitz chart, also used by Bloss (1999). (c) The quartz wedge chart by Dyar and Gunter (2007). (d) This study, the calculated chart, now used by Raith *et al.* (2012) [58]
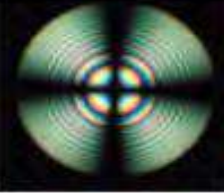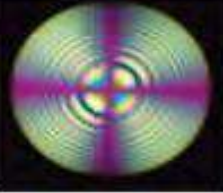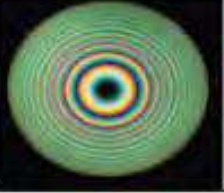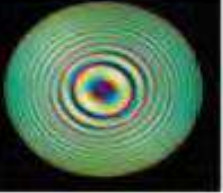
uniaxial	State of polarization of the light			
	linear		circular	
	compensator λ			
	without	with	without	with
positive quartz				
negative calcite				

Fig 3.3: Determination of the optical character of uniaxial minerals in linearly and circularly polarized light. The reference direction of the λ-compensator is aligned in NE-SW [60].

To observe the morphology via polarizing microscope the analysis was performed in the following way:

1) About 2 gm of samples was taken and grain slides were made. It was made sure that bubble formation is at minimum level and no moisture attacks the slide.

2) All sand sample were observed via polarizing microscope with magnification 2.5X, 4X, 10X to study the morphology of zircon.

Morphology also studied via SEM (JEOL JSM-7600F, SEM- Japan-2013). SEM provides information about the sample's surface topography and composition. It was performed for the as received sample to observe the size and shape.

The sample for SEM analysis was prepared in the following way:

1) Samples were adhered to the holder.

2) Samples were gone through Agar auto sputter coater.

3) They were dried and then observed via SEM.

Three-dimensional view of mineral was examined via stereo microscope. Stereo microscope includes separate objective lens and eyepiece which create two separate optical paths for each eye. The slightly different angling views to the left and right eye produce three dimensional views.

1.0gm sample was taken in slide and then observed under stereo microscope.

3.2.3 Moisture Content

The moisture content of sand is the ratio of the weight of the water present to the weight of dry sand in a given sand mass. Moisture content plays an important role in understanding the behavior of sand and clay. The property is used in a wide range of scientific and technical areas and is expressed as a ratio, which can range from 0 (completely dry) to the value of the materials porosity at saturation. Compaction of sand in the field is also controlled by the quantity of water present [60].

Moisture may be present as adsorbed moisture at internal surfaces and as capillary condensed water in small pores. At low relative humidity's, moisture consists mainly of adsorbed water. At higher relative humidity's, liquid water becomes more and more important depending on the pore size.

Due to unavailability of facilities, moisture content of sample was measured manually.

% of moisture= Weight loss of sample for 3 hours of heat / Sample Initial weight x 100

3.2.4 Particle Size Distribution

For many applications the particle size distribution of zircon is point of interest as it is important in understanding its physical and chemical properties of any material. In this work, particle size distribution was analyzed by Fritch Sieve Analysis. This technique was used because of its simplicity, cheapness and ease of interpretation. This technique was also well adapted for bulk sample.

In this experiment, a set of standard testing sieve was used to screen the sand (ASTME11). These sieves are stacked in sequence with the coarsed sieve at the top and placed in a sieve shaker. About 100.03 g sand was placed at the top sieve and after 10 minutes of vibration

at 60rpm, the weight of the sand retained in each sieve was obtained. The AFS grain fineness number of the sand was determined by taking the percentage of sand retained on each screen, multiplying each by a multiplier, adding the total, and then dividing by the total percentage of sand retained on the sieves.

AFS GNF= Total Product/ Total percentage of sand retained

The list of stainless steel-testing sieve with its size is given in Table 3.1.

Table 3.1: Testing sieve

Sl.	Sieves	Size (µ
1.	6	3.35E0
2.	12	1.70E0
3.	30	600
4.	40	425
5.	70	212
6.	140	106
7.	200	75
8.	270	53
9.	Pan	

3.2.5 Density Measurement

The density of material is one of the important and easily measured physical properties. These are widely used to identify pure substances and to characterize and estimate the composition of many kinds of mixture. It is the quantity per volume of material. The density of zircon sand is defined as the quotient mass M and volume V:

$$\rho= M/V \text{ g/cm}^3$$

The density of sand can be measured by various methods. In present experiment, the pycnometer method was used to determine the density of the sand.

In order to determine the density three parameters required-

    i) The mass of the material

    ii) The volume of the material

    iii) The temperature at which determination was carried out

Using the pycnometer method, the density of the test specimen is measured by determining the weight of a volume-calibrated pycnometer filled with a certain quantity the sample is immersed. The sample volume equals the pycnometer volume minus the displaced volume of liquid of known density. The method however requires that the liquid is used to immerse the sample be less dense and must be totally inert to the sample, i.e. the liquid must not cause any swelling or salvation of the test sample. The liquid must also be non-volatile during the course of the experiment.

In this method an empty pycnometer of 50 ml capacity (Vp) was weighed (Wp). It was half filled with zircon sand sample and was weighted (Wp + Ws). Then the density bottle was filled with distilled water and weighed (W_P+Ws+W_{rl1}). The sample of sand and water were removed and the pycnometer was again filled with water and weighed (W_P+W_{rl2}). The bulk density of the sand sample was determined as follows:

Calculation:

Weight of the solid sample, Ws= (Wp + Ws) - Wp

Weight of the liquid, Wl= (Wp + W_{rl2}) - Wp

Density of the liquid, $\rho l = W_l/Vp$

Weight of the liquid used to immerse the solid sample, Wil= (Wp+ Ws+ Wrl1)-(Wp + Ws)

Volume of the liquid used to immerse the solid sample, Vil= Wil/ ρl

Volume of the solid sample, Vs= Vp- Vil

Density of the solid sample, ρs= Ws/ Vs

The room temperature during the test was 30⁰C.

3.2.6 Phase Identification

For identification of phase or quantitative phase analysis the most widely useable tool is X-ray diffraction spectroscopy. It is a powerful nondestructive and rapid analytical technique for characterize crystalline materials. It provides information on crystal structure, phase, preferred crystal orientation, and other structural parameters like grain size, crystallinity, strain, crystal defects etc [62],

To study the crystallinity of as received and upgraded sample X-ray diffraction (XRD) was performed. The model of the machine was Rigaku Smart Lab XRD-2018. X-ray diffraction analysis is widely used in the study of sands primarily to identify the phases present in a particular sand sample.

1) The diffraction patterns were recorded in the 2θ range of 5° to 85° with a Cu Kα radiation (λ=1.5406 A$^\circ$) with an accelerating voltage of 40 KV. The step was 0.02°, step time 0.6s. The study was conducted at room temperature (25 °C). 2θ= 5.000° and θ= 2.500°.

2) The diffraction lines in the recorded patterns were matched with data in the Powder Diffraction Files of ICDD (International Center for Diffraction Data). Major peaks in the diffraction pattern were marked.

The operating conditions that were maintained during the recording of the patterns were:

   Voltage and current: 40 KV and 30 mA
   Water flow rate: 4.7 L/min
   X-ray generator source: Cu anode [Wavelength of CuKα: 1.54016 A$^\circ$]
   Window for X-ray filter: Be window

3.2.7 Dependence of Structure on Temperature

Thermo-gravimetric analysis (TGA) was performed to the zircon sample to characterize the thermal effects- to trace the loss of combined water and/or, change of polymorphic form (Model No: TGAQ50 W/FMC). The experimental setup for TGA is mentioned below:
Reference: Alumina
Reference Weight: 2.83 mg
Temperature: 30°C to 750°C at the rate of 10°C/ min

3.2.8 Surface Analysis

To analyze the surface material composition and topography SEM⁄EDX was carried out. High resolution images of surface topography, with excellent depth of field, were produced using a highly-focused, scanning (primary) electron beam. The primary electrons enter a surface with an energy of 0.5 – 30 kV and generate many low energy secondary electrons. The intensity of these secondary electrons is largely governed by the surface topography of the sample. In addition to low energy secondary electrons, backscattered electrons and X-rays are generated by primary electron bombardment. The intensity of backscattered electrons can be correlated to the atomic number of the element within the sampling volume. The analysis of characteristic X-rays (EDX or EDS analysis) emitted from the sample gives more quantitative elemental information. Such X-ray analysis can be confined to analytical volumes as small as 1 cubic micron [61].

In this study 2mm X 2 mm cross section of sand sample was taken with 100X magnification to analyze the surface composition of as received, acid leach and base leach sample.

3.3 Beneficiation

Through beneficiation processes the economic value of ore or mineral improves by removing unwanted material. In short different beneficiation technique by using higher grade product can be achieved. Based on the result of characterization, the beneficiation steps were developed. The basic beneficiation steps used in this work were acid and alkali leaching with stirring.

3.3.1 Acid Leaching

Chemical treatment such as acid washing, leaching and hot chlorination is an important addition to physical processing methods in order to achieve maximum purity zircon through the removal of surface impurities. 2M hydrochloric acid was used at 100° C for an hour with stirring. After acid leaching the sand was continued to wash several times up to achieving neutral P^{H}. Elevated temperature acid leaching is used to remove liberated surface impurities most effectively. In addition, those impurities enriched in micro fissures and dislocations, would be liberated and removed owing to an enhanced dissolution rate of zircon in regions where impurities were concentrated.

3.3.2 Alkali Leaching

Alkali leaching of sand sample is a very traditional method. This helps to eliminate certain metals from the sand surface. That's why the samples were gone through alkali leaching. NaOH was used at 250° C for production of alkaline frit (Na_2SiO_3). Na_2SiO_3 was washed consecutively up to P^H become neutral. Pure zircon was obtained after dry.

Reactions took place in alkali leach,

$$ZrSiO_4 + NaOH \xrightarrow{\quad 250^o\,C \quad} Na_2SiO_3$$
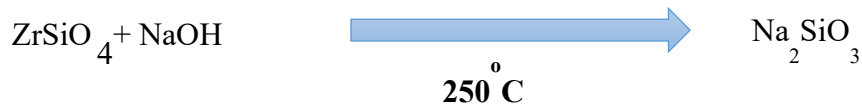
A schematic view of as received zircon beneficiation process flow chart is shown in Fig 3.4.

| As Received Sample | Acid leach with 2M HCl 100°C temp for 1 hr with stirring | Base leach with NaOH 2:1 ratio at 250°C | As Received Sample | Final Product |
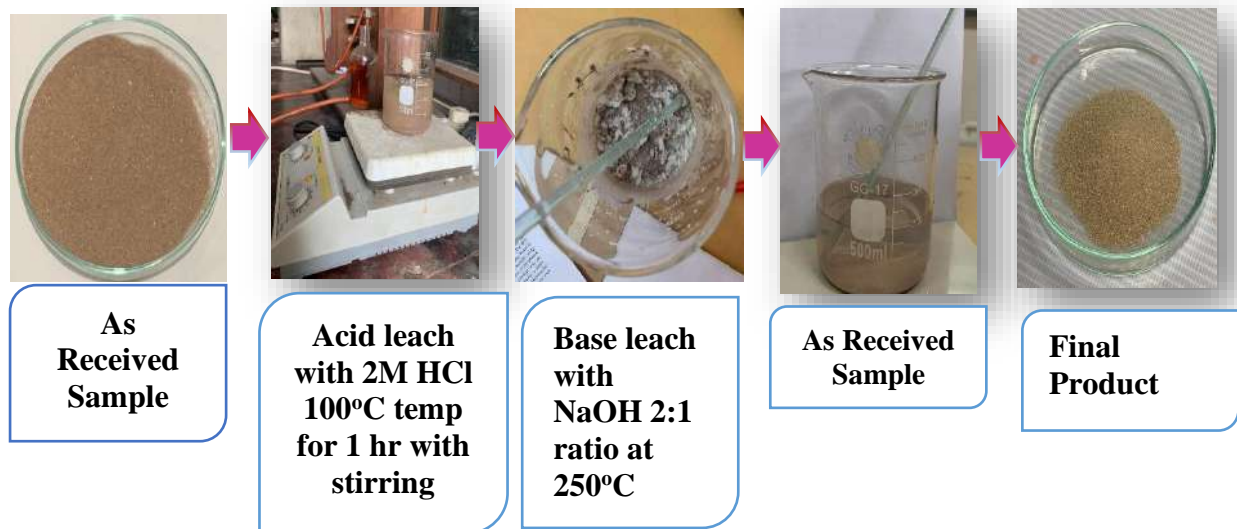
Fig 3.4: Flow chart of zircon beneficiation from raw sand

3.4 Synthesis of Nano-particle of Zircon

Different methods were used to synthesize zircon nanoparticle from zircon sand. As zircon was already in micron size top-down method had to be selected to obtain nanoforms. Mechanical method or grinding with ball mill is an old method which could successfully produce fine, uniform dispersions of oxide particles. In this process a powder mixture placed in the ball mill is subjected to high-energy collision from the balls. It is, furthermore, a way of inducing phase transformations in starting powders whose particles have all the same chemical composition: amorphization or polymorphic transformations of compounds, disordering of ordered alloys, etc [63].

The pure zircon powder was produced and then synthesized into nanometric sizes using top-down method via ball milling by varying the milling time 7.5, 10, 15, 20, 25, 30 hours followed by annealing at $200^{o}C$. Annealing was done to eliminate non-uniform residual strain in ball milled powders. In this experiment only size reduction was possible but no polymorphic transformation was observed.

Fig 3.5: Zircon nanoparticle formation by dry ball-milling followed by annealing

3.5 Synthesis of Zirconia from Zircon nanoparticle

Zirconia nanoparticle was synthesized from the extracted zircon nano powder produced by 30hours ball mill. To obtain zirconia nano-particle series of reactions were found to take place like alkali-fusion, co-precipitation, calcination etc.

3.5.1 Alkali Fusion of Zircon Nanoparticle

To do alkali fusion reaction with NaOH zircon nanopowder was mixed with NaOH in 1:2 ratio in a platinum crucible. The mixture of zircon and sodium hydroxide was heated slowly upto 80° C and kept it 15min, 120°C for 15min and at last 400°C for half an hour to remove moisture in the mixture. The sample was fused at 700°C for 3hours. Ultrasonic vibrator was used to disperse alkaline frit produced by fusion reaction. The fused product was leached and washed with di water to remove the water- soluble product. During fusion reaction four component was produced. Two of the products were removed by washing and other two remain in the solution. The reaction was:

$$ZrSiO_4 + \ NaOH \xrightarrow{700^{o}C} Na_2ZrSiO_5 \ + \ Na_2ZrO_3 + Na_4SiO_4 \ + \ Na_2SiO_3$$
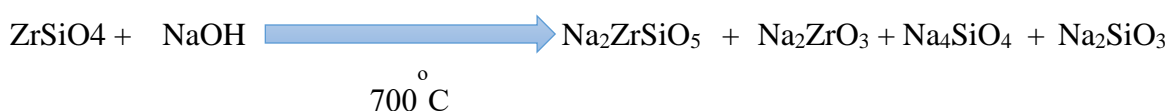
3.5.2 Co-precipitation with HCl and NH$_4$OH

Coprecipitation method is used to obtain a uniform composition in two or more cations homogeneous solution through precipitation reaction. In this system 2M HCl was used to dilute the fused product and then add 3M NH$_4$OH to get precipitation from zirconyl product. A diagrammatic flow chart of zirconia nanoparticle synthesis is shown in Fig 3.6.
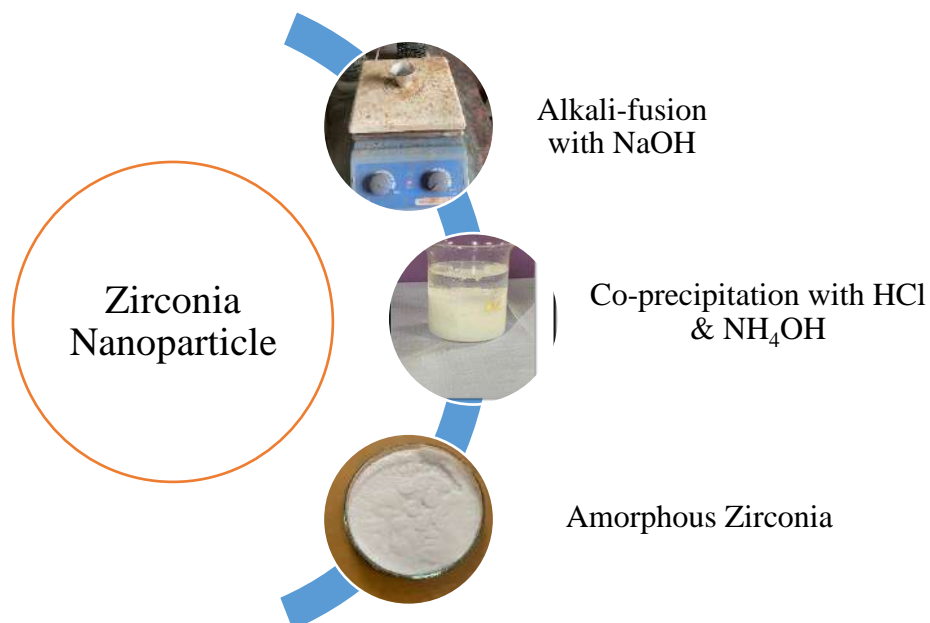
Fig 3.6: Zirconia nanoparticle synthesis

3.5.3 Crystallized Zirconia Production by Calcination

Co-precipitated zirconia was amorphous in nature. Amorphous material is thermodynamically unstable. Amorphous to crystalline transition can be induced by heat, stress or time (aging). In present case, thermal annealing was used to obtain nanocrystal from amorphous material. To obtain nanocrystal product different calcination temperatures were maintained from 800ºC-1300ºC. Depending on calcination temperatures zirconia showed different crystal structures with different texture colours as shown in Fig 3.7.
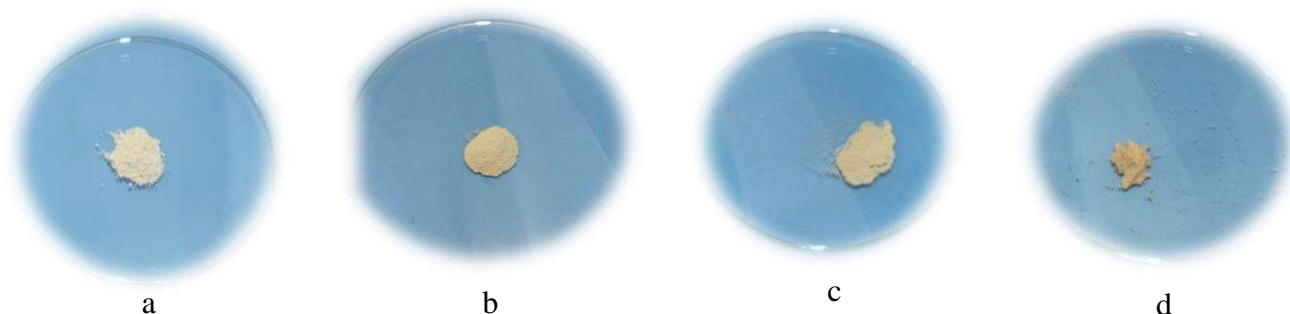
Fig 3.7: Zirconia nanoparticle obtained after different calcination temperature (a) as dried (b)1000ºC (c) 1100ºC (d) 1300ºC

3.6 Evaluation of Photocatalytic Activity

As ZrO_2 possesses wide band gap photocatalytic degradation would be observed in synthesized ZrO_2. Due to presence of silicate in $ZrSiO_4$, it does not show photocatalytic behavior. To evaluate the synthesized zirconia photocatalytic property, methylene blue dye was used. Decolorization of MB was observed by UV-vis spectroscopy. UV-Vis spectroscopy is an analytical technique to measure the amount of discrete wavelengths of UV or visible light that are absorbed by or transmitted through a sample in comparison to a reference or blank sample [63]. This property is influenced by the sample composition, concentration etc.

In this study 0.01mM MB was used. The sample suspension was formed by adding 1.0 mg zirconia sample in 50ml solution. Before photoreaction, the suspension was magnetically stirred in dark for 30 minutes in room temperature to establish adsorption-desorption equilibrium between dye molecules and photocatalyst surface. The suspension was irradiated with three UV lamps while being stirred continuously. The degradation of dye measured at first 30min adsorption under dark. The same surface, without UV irradiation, was served as reference. Throughout the measurement, the colour concentration of the solution was measured by UV-vis spectroscopy (Model: UV1800, UV-Vis Spectrometer, frequency 50, Shanghai UPG International). The experimental flowchart and schematic view of MB photodecomposition is shown in Fig. 3.8.
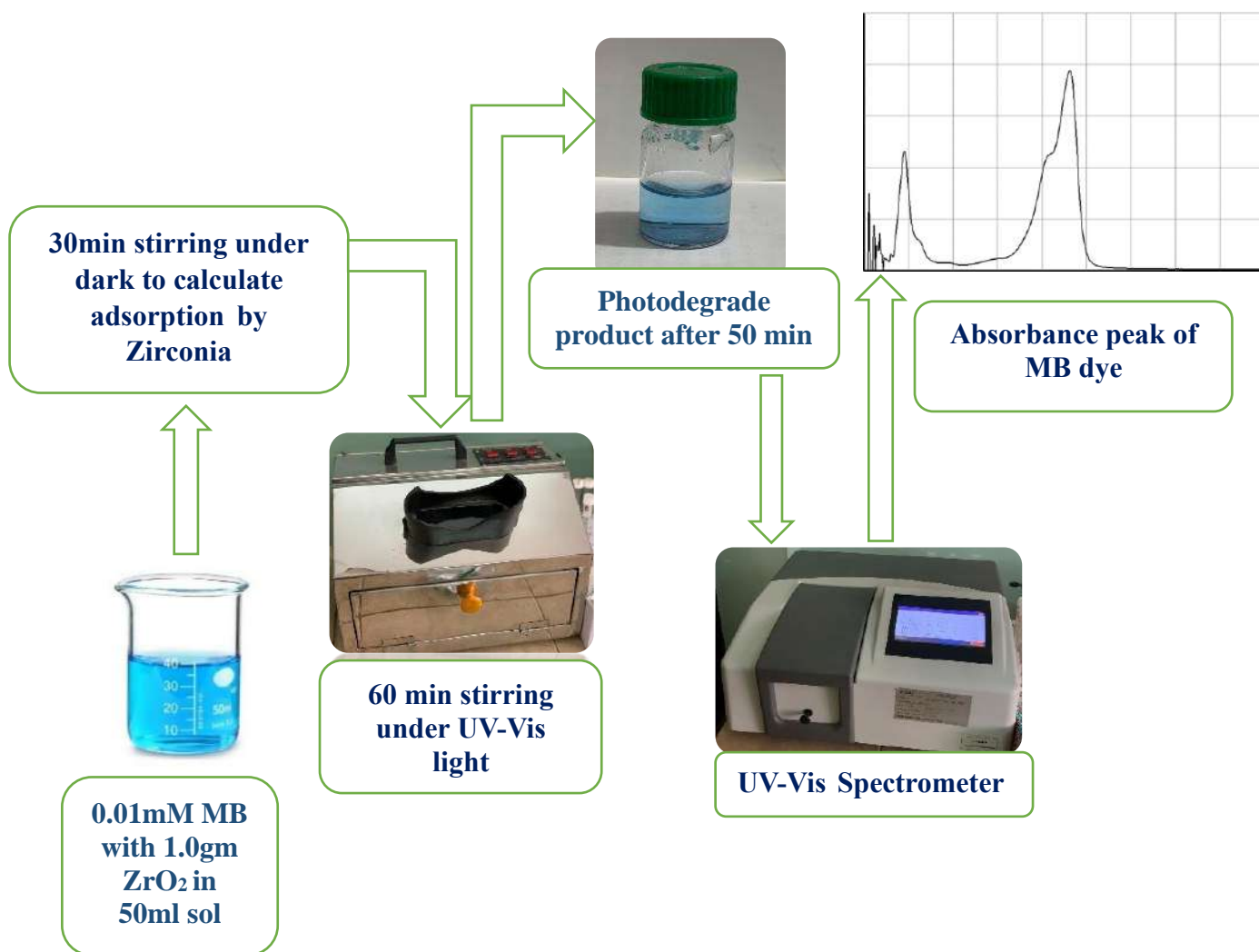
Fig 3.8: Flowchart of MB photodecomposition experiment by ZrO_2 nanoparticle.

Results and Discussion

4.1 Sample Selection

Based on the characterization sand samples were ranked according to the prospect of use in high tech applications. Sand sample was collected from Cox's Bazar beach sand. Selected sample would undergo characterization and further beneficiation process. Location of the selected sample is shown in the map in Fig 4.1. According to GPS coordinates of Cox's Bazar beach latitude and longitude is 21.5833 and 92.0167 respectively.
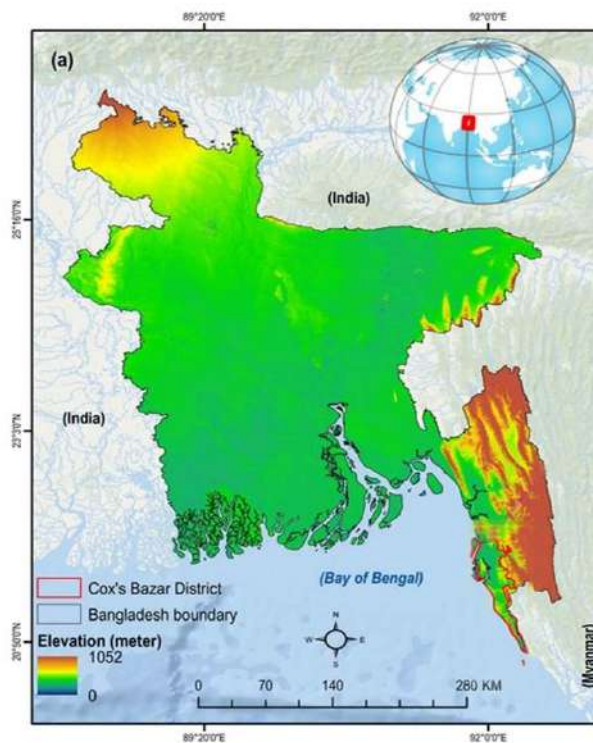
Fig 4.1: Location of collected sample

4.2 Characterization

All the experimental results of as received and upgraded samples about mineralogy, chemistry and physical properties are discussed in the subsequent sectors. The results on characterization parameters like composition, size, density, transportation, moisture content, material composition, crystallinity, morphology, surface analysis, particle size distribution etc are shown below.

4.2.1 Material Composition

The mineralogy of the material was examined by XRF before and after upgradation. The chemistry and composition of the sample can be well understood from Table 4.1.

Table 4.1: Sand sample composition before and after beneficiation (XRF Analysis)

Analyte	Raw Sample		Acid Leach		Acid+Base Leach	
ZrO_2	83.7831	94.78	73.7634	95.3544	76.5076	95.62
SiO_2	11.000		21.5904		19.1122	
TiO_2	3.8204		3.3918		3.0103	
CaO	.4061		.2560		.5661	
Y_2O_3	.2858		.2236		.2352	
Fe_2O_3			.1765		.1364	
P_2O_5	.1864		.1351		.1257	
Al_2O_3	.2912		.1992		.1245	
Er_2O_3	.1196		.1114		.1145	
K_2O	.1074		.0848		.0676	

The XRF result shows that main impurity of the sand sample was rutile which decreased from 3.8% to 3.39 % after acid leach and after base leach the content decline to 3.01%. As XRF showed results in oxide form zircon upgradation, result should not come to an end by analyzing this result. Other undesirable analyte also decreased after upgradation.

4.2.2 Morphology

The morphology of as received sample was studied by SEM. The colour, size and shape of the minerals before and after beneficiation were also studied under stereo and polarizing microscope.

4.2.2.1 Morphology Study by SEM

Morphology was studied under scanning electron microscope (SEM) where 100, 200,300 and 500 magnifications were used. Hexagonal, pyramid, elliptical shaped zircon was found under SEM as shown in Fig 4.2. The size of particles was also measured under 100X magnification of SEM as stated in Fig 4.3. The maximum size of zircon was measured which was cylindrical in shape (272µm). Minimum size was 105 µm and was spherical in shape. As discussed earlier being igneous rocks zircon showed different shapes due to recrystallization or corrosion during transportation and weathering process.

(a)　　　　(b)　　　　(c)　　　　(d)
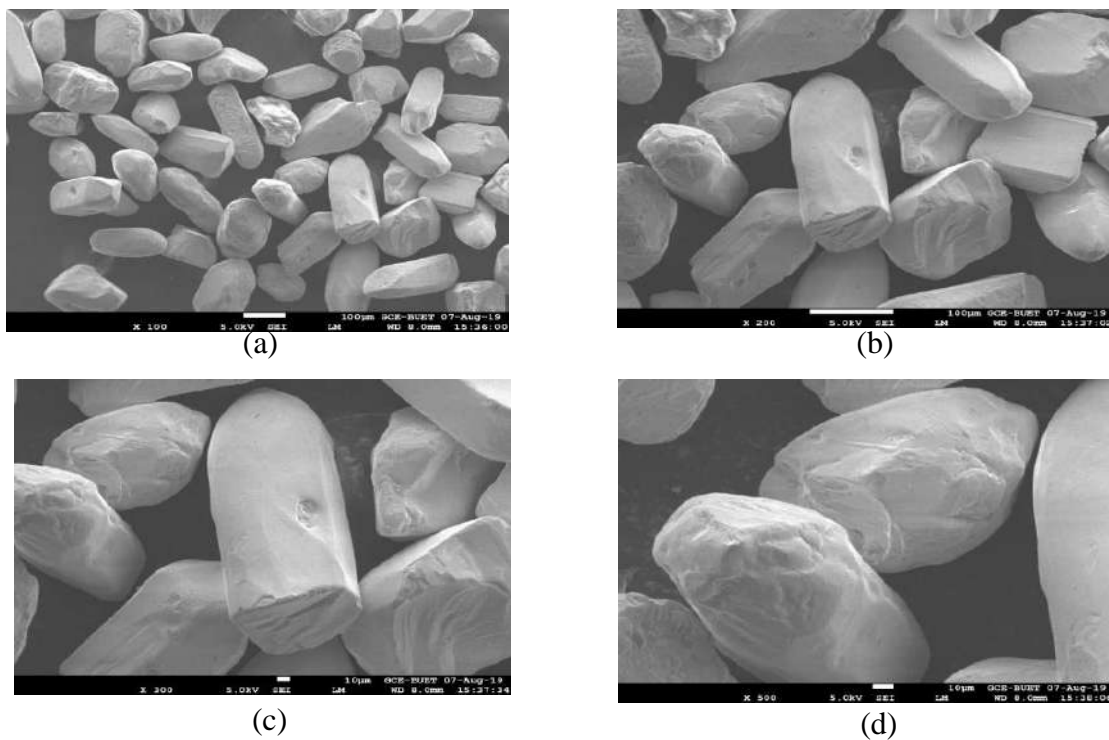
Fig 4.2: SEM image under different magnification (a) 100X (b) 200X (c) 300X (d) 500X
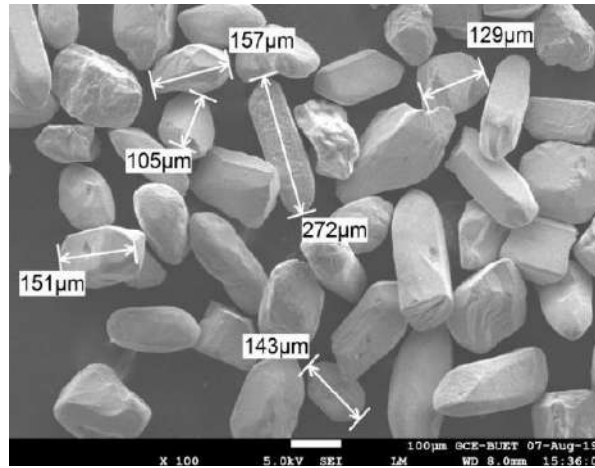
Fig 4.3: Size measurement by SEM under magnification 100X

4.2.2.2 Morphology Study by Stereo Microscope

(a)

(b)

(c)
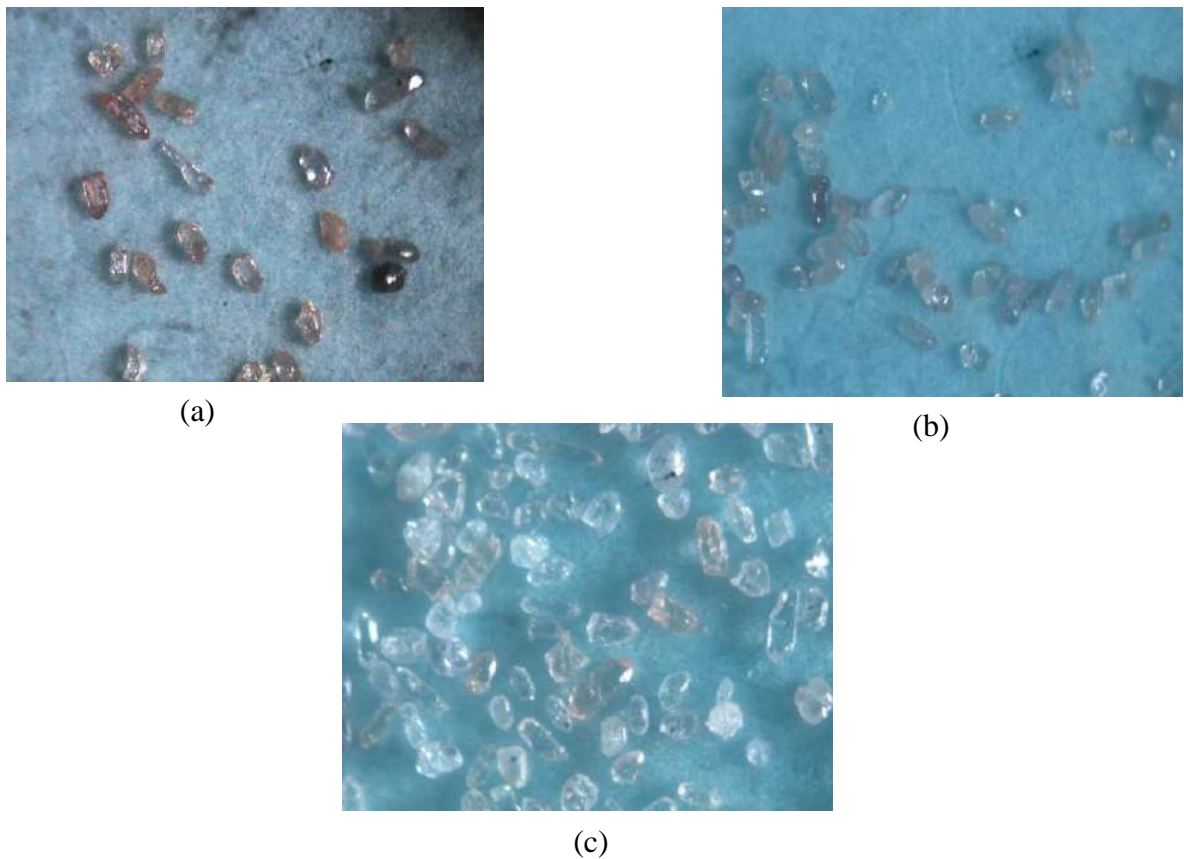
Fig 4.4: With spot magnification of 100X stereo microscope view of (a) As received sample (b) Sample after acid leached (c) Sample after base leached

Stereo Microscopy carried out under 100X mgnification. Here beneficiation processes showed removal of inclusion from external surface. This was clearly observed under

microscope before and after beneficiation. The maximum size of zircon was observed 178 µm.

4.2.2.3 Morphology Study by Polarizing Microscope

Fig 4.5 showed polarizing microscopic view under plane and cross polarized light of as received sample.

| (a) | (b) | (c) |

| (d) | (e) | (f) |
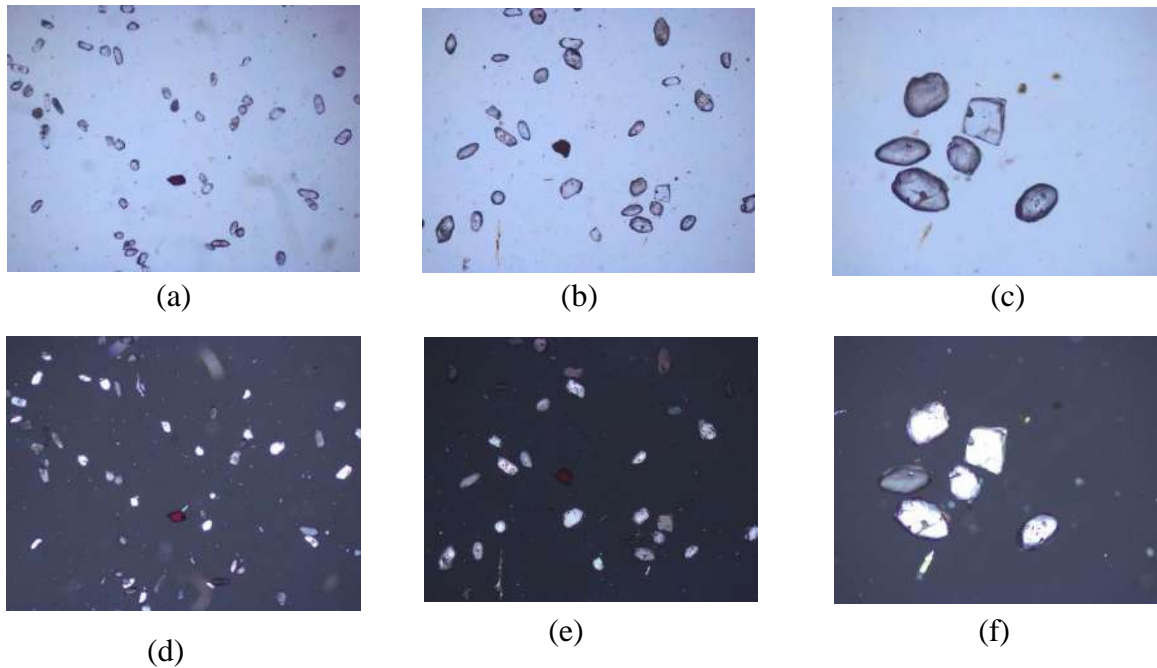
Fig 4.5: Polarizing microscopic view of as received sample under different magnification (a) 2.5X (b) 4X (c) 10X (plane polarized) and (Cross polarized) (d) 2.5X (e) 4X (f) 10X

Polarizing microscopic view under cross polarized and plane polarized light of upgraded sample after acid leaching under different magnification is shown in Fig 4.6.

| (a) | (b) | (c) |
| (d) | (e) | (f) |
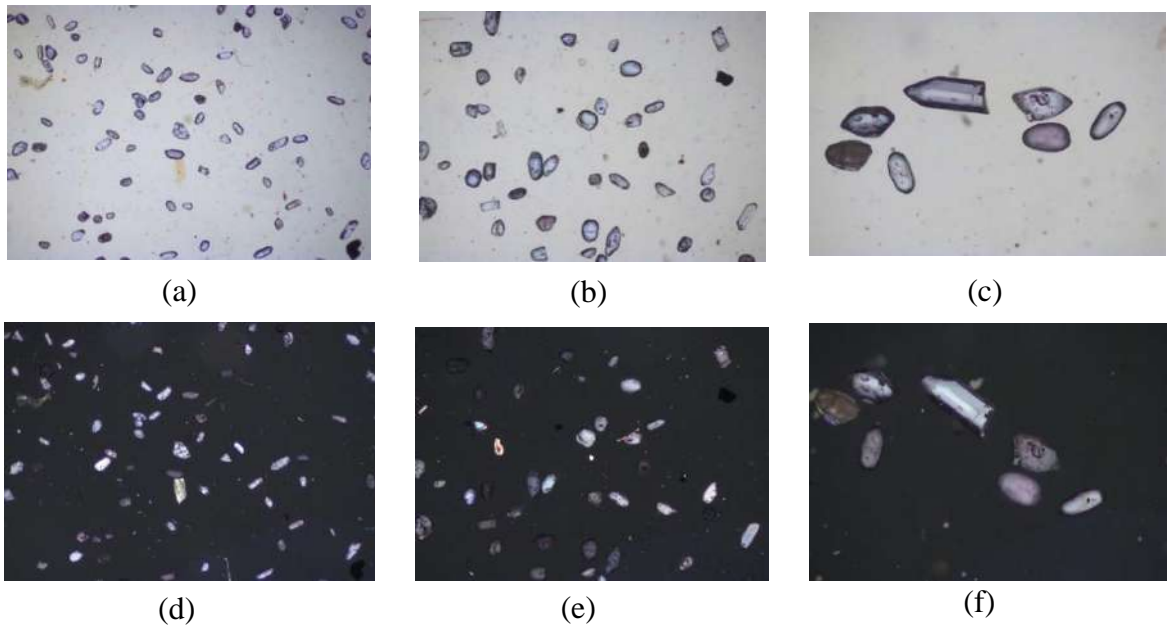
Fig 4.6: Polarizing microscopic view of acid leached sample under different magnification (a) 2.5X (b) 4X (c) 10X (plane polarized) and (Cross polarized) (d) 2.5X (e) 4X (f) 10X

At last polarizing microscopic view under cross polarized and plane polarized light of upgraded sample after alkali leaching under different magnification is shown in Fig 4.7.

| (a) | (b) | (c) |
| (d) | (e) | (f) |
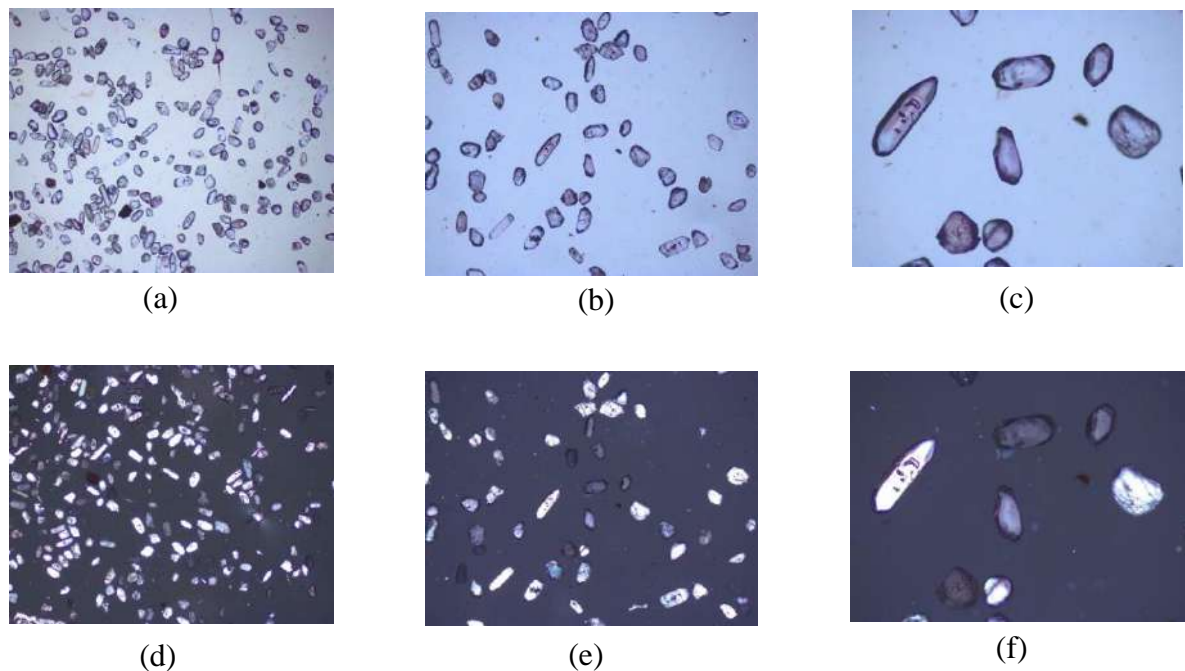
Fig 4.7: Polarizing microscopic view of alkali leached sample under different magnification (a) 2.5X (b) 4X (c) 10X (plane polarized) and (Cross polarized) (d) 2.5X (e) 4X (f) 10X

Morphology was studied under polarizing microscope. Plane and cross polarized light were used to observe a clear picture. 2.5, 4 and 10 magnifications were used. Zoned zircon was observed in some zircon particle but in very minute amount. So, some of the zircon particles were expected to crystallize from ancient magma. Inclusions were also found in zircon particle.

4.2.3 Moisture Content

For the beneficiation process in further stages (e. g. high tech application), one must ensure no presence of water because small amount of water have an enormous fluxing effect-it lowers the melting point. The as received sample contained only 0.4% of moisture which was negligible in amount.

4.2.4 Particle Size Distribution

In this work, particle size distribution is analyzed by Fritch sieve analysis.

Table 4.2: Sand sample sieve analysis

Mesh Size	Weight(gm)	% of Sand Retained(A)	Multiplier(B)	Product (A x B)
40	.011	.011	30	.33
70	.033	.033	50	1.65
100	2.9694	2.97	72	213.84
140	71.4138	71.41	100	7141
270	25.4371	25.44	200	5088
Total	99.86	100		12444.82

AFS Grain Fineness No = 124.62

During the experiment, mesh 6, 12, 30 didn't contain any particle. AFS grain fineness number 124.62 resembled that the particles of sand sample were uniformly distributed.

4.2.5 Density Measurement

Wt of the sample = 8.24 gm

Weight of the liquid used to immerse the solid sample,

Wil= (Wp+ Ws+ Wrl1)-(Wp + Ws)

=85.99-38.41 gm

=47.58 gm

Vol of Pycnometer= 50ml

Wt loss of water =(50-47.58) gm

=2.42gm

Density of the sample is 3.41 gm/ml

The density of as received zircon sand was 3.41 gm/ml which varies from standard value of pure zircon (3.9-4.8 gm/ml). This deviation may be due to presence of inclusion on particle surface and presence of rutile.

4.2.6 Dependence of Structure on Temperature

TGA was performed to raw sample to characterize the thermal effects- to trace the loss of combined water or change the polymorphic form.
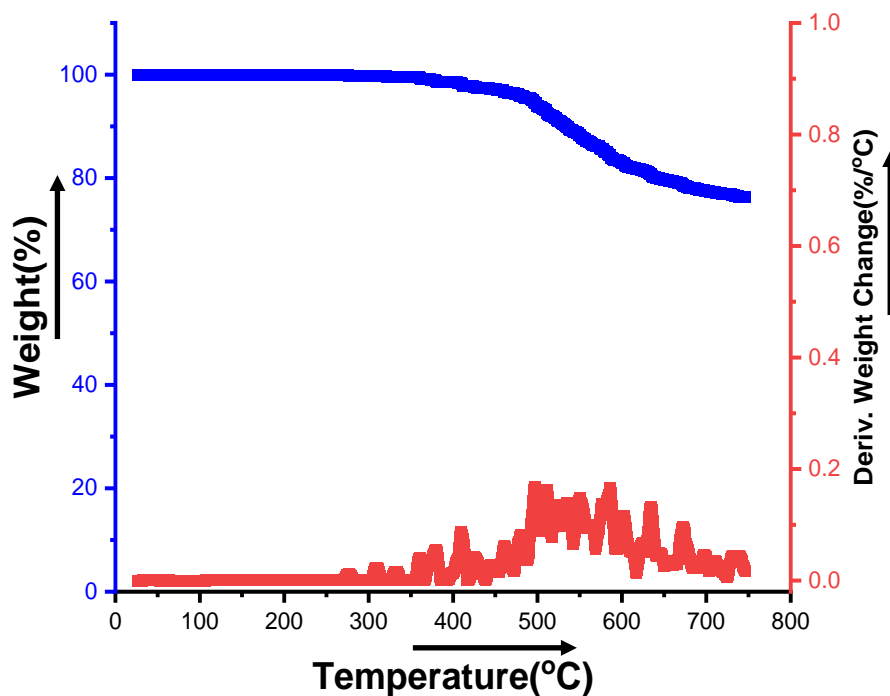
Fig 4.8: Thermogravimetric Analysis (TGA) of as received sample showed no phase change between $0^{o}C$ to $750^{o}C$

Within present available facilities in TGA, only $0^{o}C$ to $750^{o}C$ temperature could be varied. Within this temperature range no phase change was obtained.

4.2.7 Surface Analysis

SEM/EDS is a surface analysis tool. It was used to analyze the surface. It can create elemental maps of the surface. Depth information can also be found by using variable excitation voltage. Here sectional method was used. Fig 4.9 showed the analysis results before and after upgradation. Fig 4.9 (a) showed elemental Ti peak but after acid and base leach no such peak was found which were shown in Fig. 4.9 (b) and 4.9 (c) respectively.

(a)

(b)

(c)
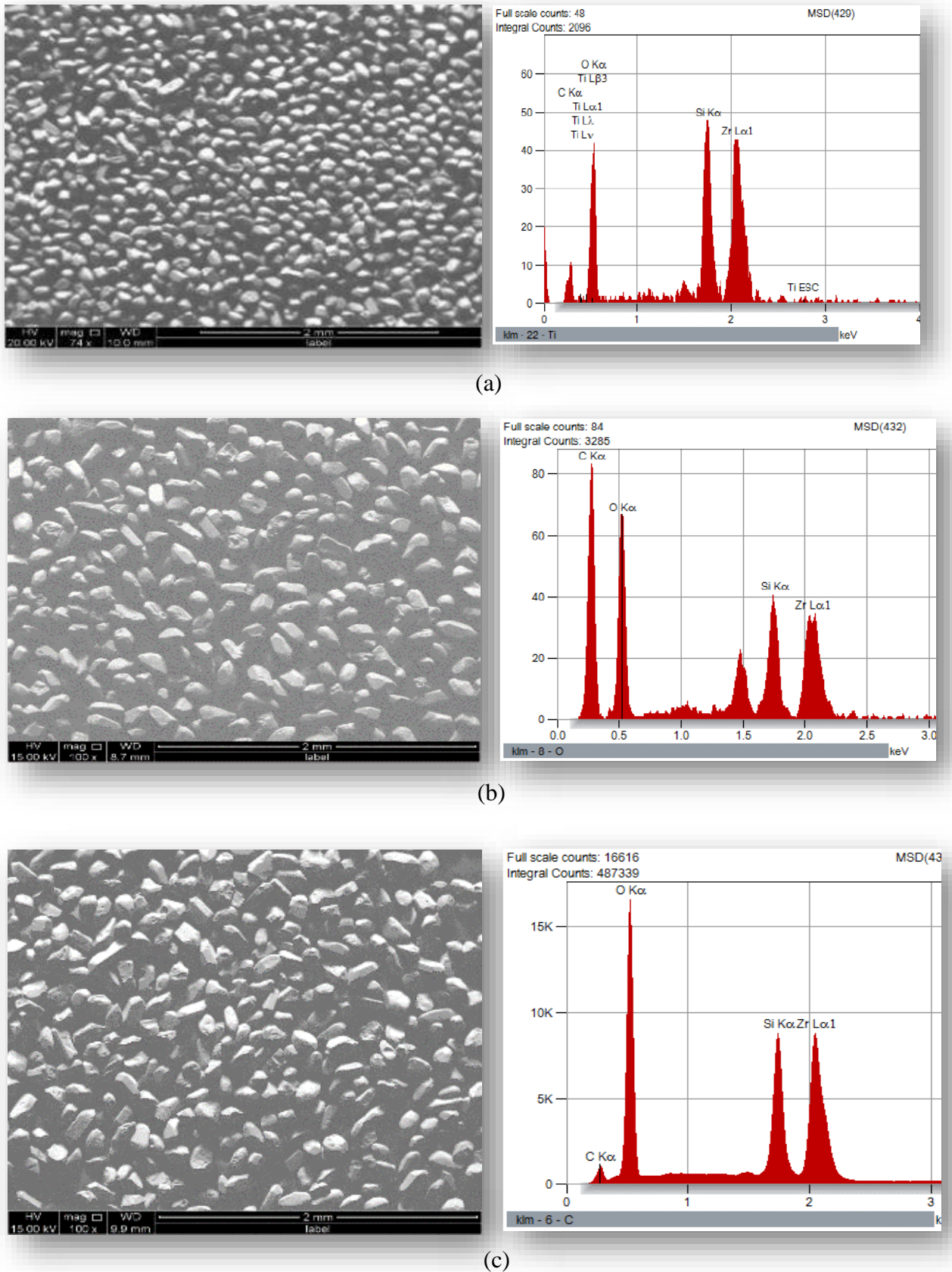
Fig 4.9: SEM/EDS result of (a) as received (b) acid leached (c) alkali leach sample within $2 \times 2mm^2$ cross section sample under 100 X magnification

65

Table 4.3 showed the analytical result. By observing this result, it could be explained that rutile, the main impurity completely diminished after beneficiation process as elemental Ti was not found in 2X2 mm^2 after beneficiation. Elemental Si % increased may be due to reaction of zircon with caustic soda. Elemental C is shown the Table 4.3. This elemental C was for carbon tape which was used in SEM/EDS analysis which was not the element of raw or upgraded sample. Elemental Zr yield was also increased from as received (34.64%) to upgraded sample (37.96%).

Table 4.3: Quantitative result of SEM/EDS within 2 X 2mm^2

Element	Weight (%)		
	As Received	Acid Leached	Acid+Base Leach
C	8.79	27.07	2.85
O	38.49	41.59	47.05
Si	12.61	0.00	12.13
Ti	5.47	-	-
Zr	34.64	31.34	37.96
Total	100	100	100

4.2.8 Phase Identification

To study the crystallinity of the sample before and after beneficiation XRD was carried out.
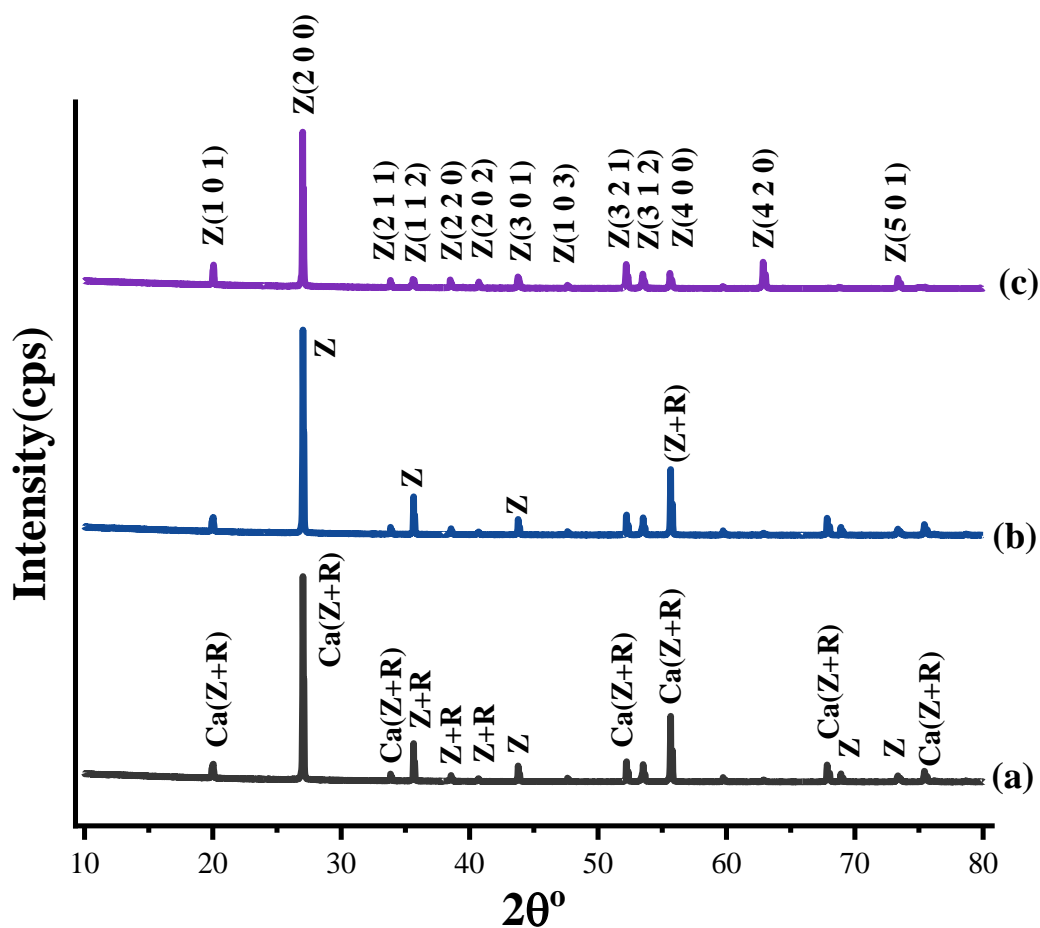
Fig 4.10: XRD results of sand samples of (a) as received (b) acid leached (c) acid+ base leached. $\lambda=1.5406$ A^o. Z= tetragonal $ZrSiO_4$ with a=6.59876, b= 6.59876, c=5.97907, $\alpha=\beta=Y=90^o$, R= tetragonal TiO_2 with a= 4.66902, b= 4.66902, c= 2.99150, $\alpha=\beta=Y=90^o$. Ca(Z+R)= Titanite Zirconian Ca (Ti0.47 Zr0.5).

Fig 4.10 showed the XRD pattern of as received, acid and base leached sample. Without any treatment as received sample showed mostly tetragonal zircon. The main impurity of this sample was found rutile. Other impurity was compound of calcium and silica. Through

Reitveld analysis it was found that about 73.8% sand sample contained zircon whereas 19.8% was rutile and 6.4% was a compound of calcium silicite.

After acid leach complete removal of rutile was obtained but increase of silicate compound was remarkable (15.8%). 84.2% purity was achieved via acid leach. However, after alkali leach 86.3% purity was achieved through removal of silicite complex of calcium.

4.3 Beneficiation

The aim of the beneficiation process was to increase zircon yield. Reitveld analysis tool was employed in XRD data to obtain crystalline phase percentages. The analysis is appended in Table 4.4

Table 4.4: Reitveld analysis result of XRD pattern of sand sample before and after beneficiation

Phases	Zircon Tetragonal (ZrSiO₄) %	Rutile (TiO₂) %	Calcium Catena Silicate (CaSiO₃) %
As Received	73.8	19.8	6.4
Acid Leach	84.2	0.0	15.8
Acid + Base Leach	86.3	0.0	13.7

Through leaching with HCl rutile was removed completely from zircon. This was happened due to presence of hot HCl with continuous stirring.

In alkali leach, NaOH fused with zircon sand at 250°C which produced alkaline frit. The yield was not increased significantly. This might be happened because all zircon sand could not take part in the fusion reaction to form caustic frit.

Naher and Haseeb, 1997, Naher and Haseeb, 2000, Naher and Haseeb, 2006 *et al.* [56] could achieved 95.88% pure beach sand zircon with 3.01% rutile. In this case, though the purity could be achieved only 86.3%, complete removal of rutile was possible through acid and base leach.

4.4 Synthesis of Nano-particle of Zircon

4.4.1 Effect of Milling Time on Nanoparticle Formation

The upgraded zircon powder was processed into zircon nanopowder using a milling and annealing method. Fig. 4.11(a) shows that no phase change was observed after 30 hours of dry ball mill. Fig 4.11 (b) showed the broadening characteristic of un-milled and milled powders which indicates the effect of milling and annealing. Saravanam *et.al* [63] showed that in ball milling when crystal size was reducing, number of various defects and dislocations were increasing which breaks the long-range symmetry of crystal lattice and redistributed the scattering intensity. The broadening of the XRD peak is mainly due to the nanometric crystallite size and the presence of non-uniform strain evolve from various dislocations.
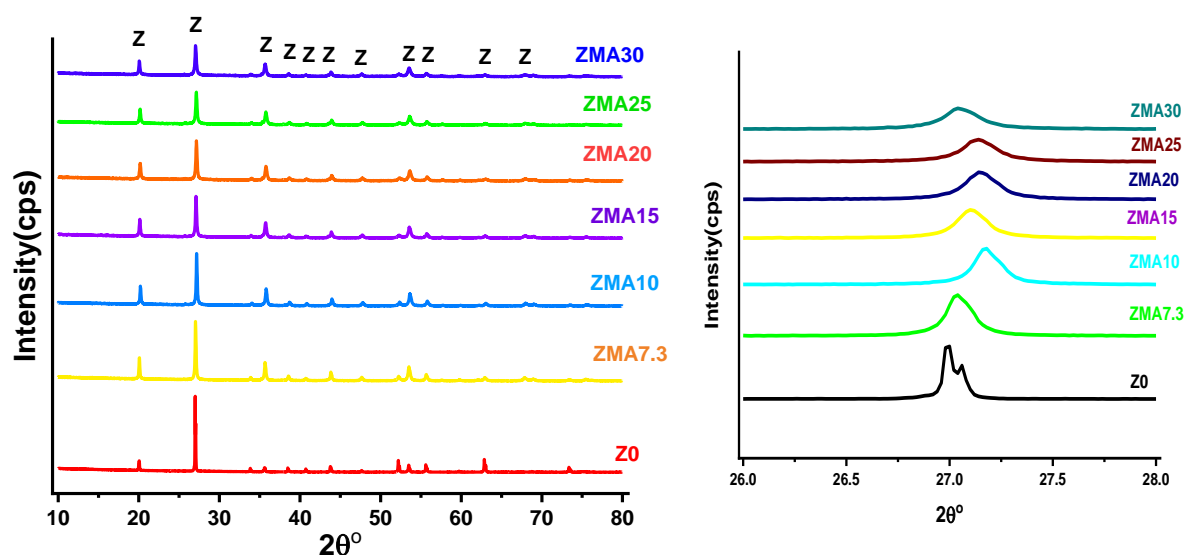
Fig 4.11: (a) X-Ray diffraction patterns (CuKα) of sample ZMA (milled-zircon powder with anneal) with variation of milling time for 0–30 h (b) XRD peak broadening details of 0 h and 30 h Symbols: ZMA = Zircon (ZrSiO$_4$) Milled sample with annealing.

4.4.2 Effect of Milling Time on Particle size and Microstrain

By using Scherrer Equation, crystal size was calculated.

$$D = \frac{K\lambda}{\beta \cos\theta}$$

D is the Crystallite size for $\leq$ 200nm

K= Scherrer constant .94 for spherical

λ is the Wavelength of X-ray. CuKα =1.5406 A^o

β is the line broadening at FWHM in radians.

θ is the Bragg's angle.

Nanoparticle started to form after 10 hours of ball milling. After 30 hours of ball mill 51.04 nm particle size could be achieved. Fig 4.12 shows the changes in crystallite size and microstrain with change of milling time. From curve, it was found that crystal size decline sharply after 10 hours of ball mill and leveled off between 15 hours to 30 hours. This result can be described as follows: in the early steps of the milling, intensive stresses result in an increasing dislocation density inside the crystals. Lestary and Dwi *et al.* [3] showed that prolonged milling causes increases in lattice strain which results in a crystal disintegration into smaller crystals with a lower strain. Further milling did not significantly change the zircon crystallite size as because due to extensive milling causes plastic deformation for excessive heat rise. Plastic deformation and dislocation motion were being active at the same time. Therefore, decreasing the zircon crystallite size was effective during the first 10 h of milling and after that collisions of balls in the zircon powder were no longer able to produce crystal disintegration in significant amount [3].

On the other hand, microstrain behaves inversely to the crystallite size (Fig. 4.12). 2 hours annealing at 200ºC could not remove residual stain. Rather with increasing milling time microstrain was found to be increased. Micro-strain was calculated by using following equation.

$$\text{Microstrain } \varepsilon = \frac{\beta}{4\tan\theta}$$

The strain calculated after 10hr, 15hr,20hr, 25hr and 30 hr were 1.9 x 10^{-3}, 2.45 x 10^{-3}, 2.75 x 10^{-3}, 2.81 x 10^{-3}, 2.99 x 10^{-3}, respectively. M. Lestari *et. al* [3] explained that, strain increase due to collision and friction between balls and zircon particles. Moreover, with increase of milling time dislocation density increase thus increase localized stress. So, overall microstrain increase with decrease of crystallite size.
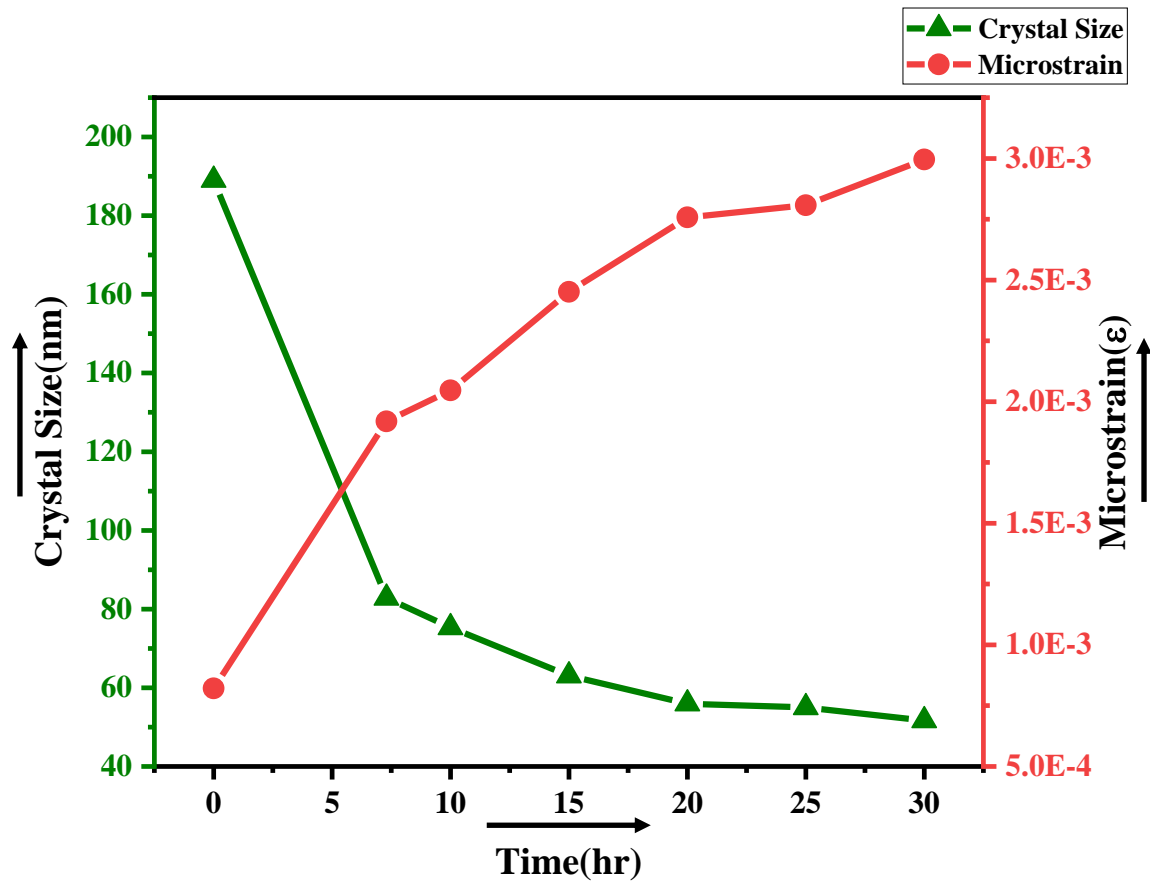
Fig 4.12: Effect of milling on crystallite size and strain of zircon powders. The reported values were extracted from milled samples followed by annealing (ZMA) at 200 °C for 2h

4.5 Synthesis of Zirconia from Zircon nanoparticle

4.5.1 Effect of Calcination Temperature on Degree of Crystallinity

Zircon nanoparticle after alkali fusion with NaOH and co-precipitation with HCl and NH$_4$OH, amorphous zirconia was formed. By using XRD pattern crystal structure was studied. Degree of crystallinity was measured with the help of following equation.

$$\text{Degree of Crystallinity} = \frac{\text{Area of all crystalline peaks}}{\text{Area of all amorphous and crystalline peaks}} \times 100$$
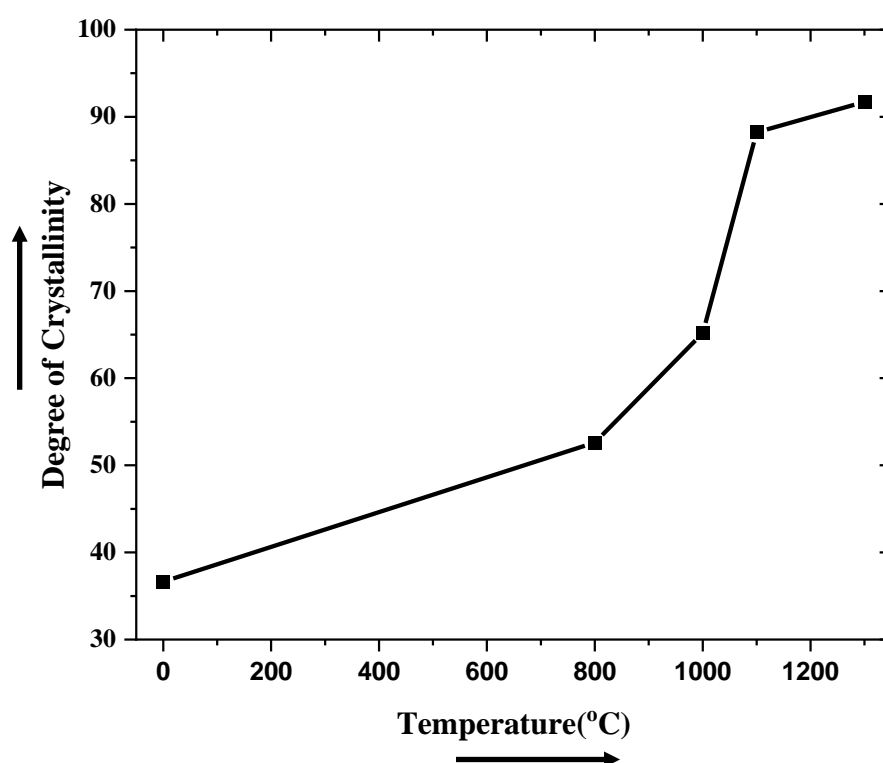
Fig 4.13: Effect of calcination temperature on degree of crystallinity.

Fig 4.13 showed the calcination temperature effect on degree of crystallinity. As calcination temperature increase, degree of crystallinity was found to be increased. As dried sample showed 36.63% crystallinity which may be due to undecomposed zircon. In fusion reaction all zircon might not undergo reaction with NaOH due to agglomeration which showed some degree of crystallinity in amorphous zirconia. Increase of temperature upto 1300°C increase the crystallinity 91.7%.

4.5.2 Effect of Calcination Temperature on ZrO₂ Crystal Structure
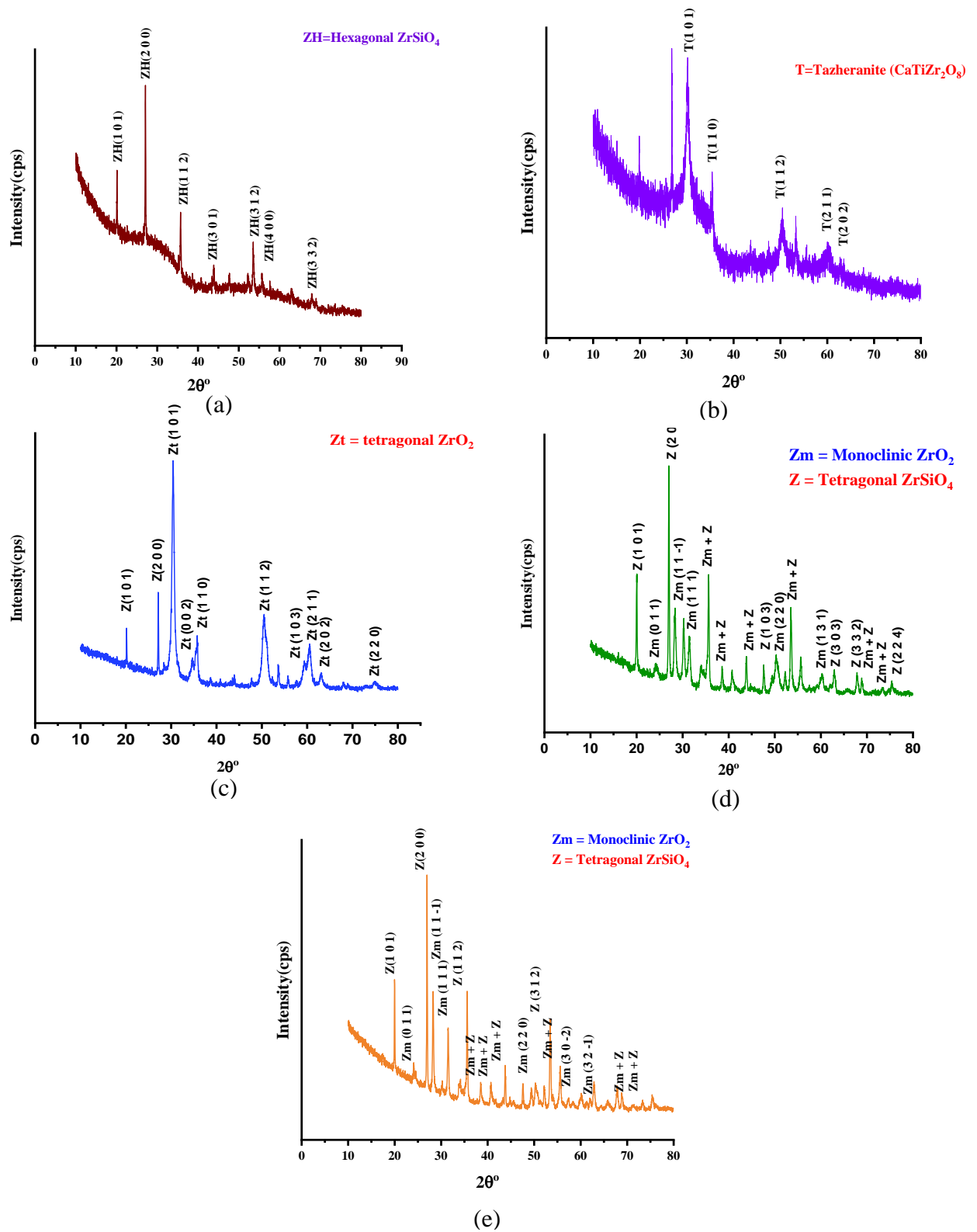
Fig 4.14: XRD pattern of zirconia nanoparticles at different calcination temperatures (a) as dried (b) 800ºC (c) 1000ºC (d) 1100ºC (e) 1300ºC

Fig 4.14 showed XRD pattern of as dried and calcined sample of 800ºC, 1000ºC, 1100ºC and 1300ºC of synthesized ZrO_2. As dried sample showed hexagonal structure of zircon which may be due to the fusion reaction with NaOH. Chau *et al.* [60] showed that during multiple nucleation each tetragonal crystal generates several twinned hexagonal crystallites with different crystallographic orientations which reveal twisting of the crystal lattice about the *c*-axis. The residual stress present in the material was not enough for the nucleation of stable phase. With increasing calcination temperature hexagonal $ZrSiO_4$ transformed to its own tetragonal structure which was a stable phase. Amorphous ZrO_2 was not shown in XRD pattern. On the other side, with increase of calcination temperature crystallinity was increased as shown in Fig 4.13. Tetragonal ZrO_2 was found to be formed at 800ºC. Crystallized ZrO_2 at 1000ºC temperature was mostly tetragonal in nature. By observing the XRD pattern of ZrO_2 at 1100ºC and 1300ºC it was found that it was a mixture of monoclinic and tetragonal zirconia. By observing the colour of synthesized ZrO_2, it was found that as dried sample was completely white in colour. With increase of temperature colour of ZrO_2 was becoming dark brown.

Table 4.5: % of crystalline phases at different calcined temperature calculated by Reitveld analysis

Phases	Calcination Temperature				
	As Dried	800ºC	1000ºC	1100ºC	1300ºC
Zircon (Hexagonal)	85.0%	21.6%			
Zircon (Tetragonal)			12.1%	55.1%	57.3%
Zirconia (Tetragonal)	8.3%	59.6%	78.7%	12%	.9%
Zirconia(monoclinic)			2.6%	25.5%	38.4%
Zirconia (Cubic)			6.4%	6.4%	.5%
Quartz	6.7%	18.8%	.1%	1%	2.9%

By observing Table 4.5, it was found that monoclinic structure increase with increase of calcination temperature. At lower temperature most of the zirconia was tetragonal structure. Cubic zirconia formed at 1100ºC and 1000ºC (6.4%). Undecomposed zircon showed hexagonal structure at as dried condition and 800ºC calcined temperature but at higher calcination temperature there was non-existance of hexagonal zircon rather the undecomposed zircon turned to tetragonal in structure. Maximum tetragonal zirconia was

found in 1000ºC and maximum monoclinic zirconia was shown at 1300ºC. No monoclinic and cubic zirconia was found before 1000ºC calcination temperature. Through fusion reaction with NaOH, SiO_4^- should be removed from zircon. But complete removal of SiO_4^- was not possible rather it remained in the sample as quartz.

4.6 Evaluation of Photocatalytic Activity

4.6.1 Effect of calcination temperature on photodecomposition

Photocatalytic activity of ZrO_2 nanoparticles synthesized at different calcination temperature was determined by monitoring the degradation of MB dye. Fig 4.15 shows the changes of absorbance spectra of MB solution (00.01mM) at 60 minutes irradiation interval of different ZrO_2 nanoparticle sample. Degradation of 0.01mM MB dye was strongly dependent by calcination temperature of synthesized ZrO_2. Major absorbance peak of MB dye was found in 664nm due to benzene ring and hetero-polyaromatic linkage. This absorbance peak showed little feebleness after 60 minute of treatment time in case of as dried sample. As dried sample consisted little amount of crystallized zirconia. Only crystalline phase in this sample was hexagonal zircon which has no capability to take part in photocatalytic reaction.
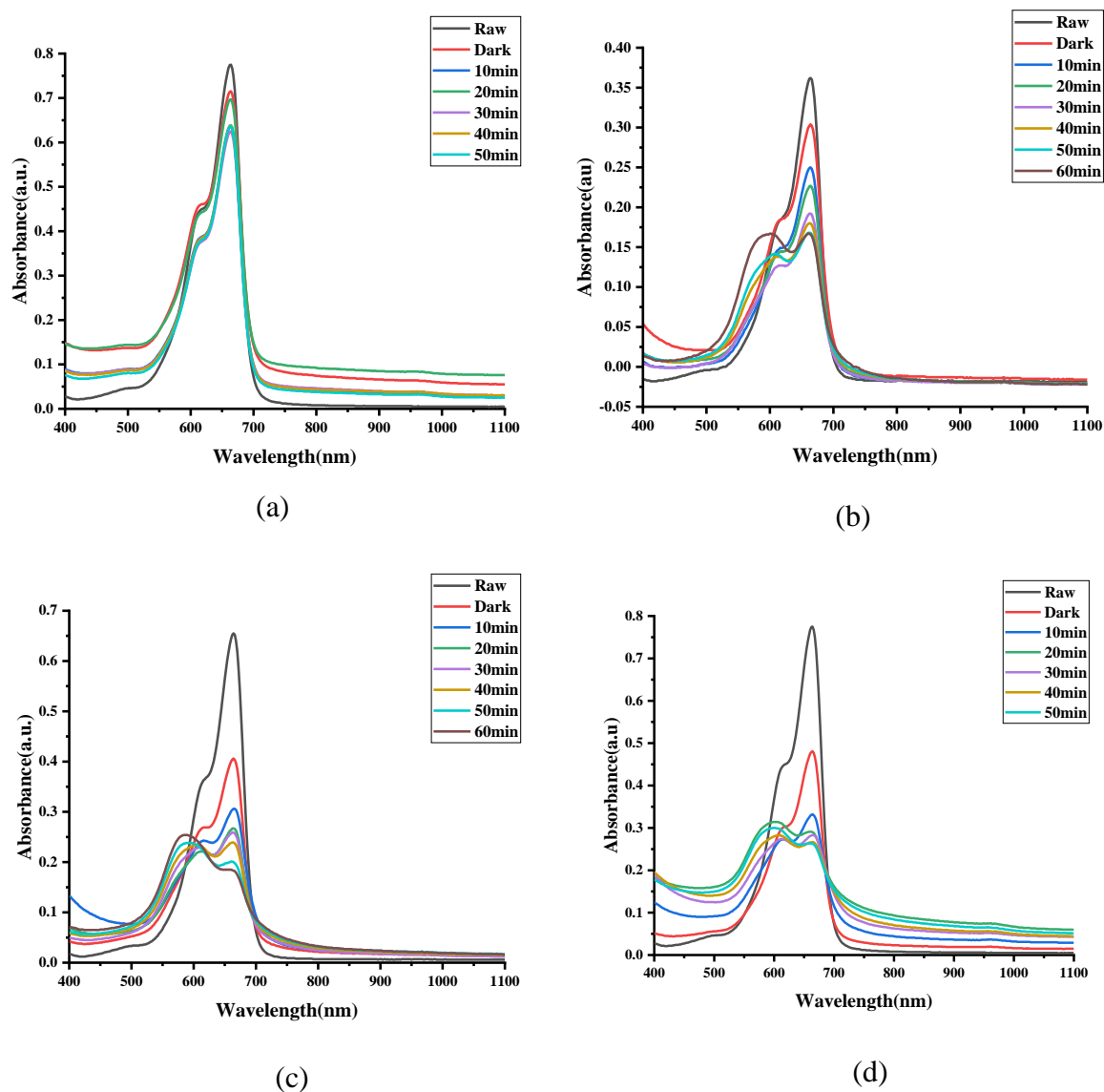
Fig 4.15: Absorbance spectra of photocatalytic degradation of ZrO_2 nanoparticle at different calcined temperature (a) as dried (b) 1000°C (c) 1100°C (d) 1300°C

Absorbance found to be diminished slowly when calcination temperature of synthesized zirconia increased. The decrease in the absorbance spectra was due to the destruction of the homo and heteropolymeric rings present in MB [66]. Adsorption-desorption equilibrium was prominent in case of all calcined sample. In case of 1000°C, 1100°C, 1300°C calcined temperature samples 16.02%, 38.01% and 38.2% adsorption could be achieved respectively. So, adsorption capability increased with increasing calcination temperature.

With increase of calcination temperature monoclinic ZrO_2 synthesis increased as such adsorption is higher in 1300ºC than 1000ºC and 1100ºC temperature calcined sample.

4.6.2 Effect of calcination temperature on decolorization efficiency

The decolorization of 00.01mM MB was calculated with 60 minutes duration as shown in Fig 4.16. It was found that degradation was minimum for as dried sample and degradation was maximum at 1100ºC calcined temperature. As stated earlier, with increasing temperature percentage of monoclinic structure increased.
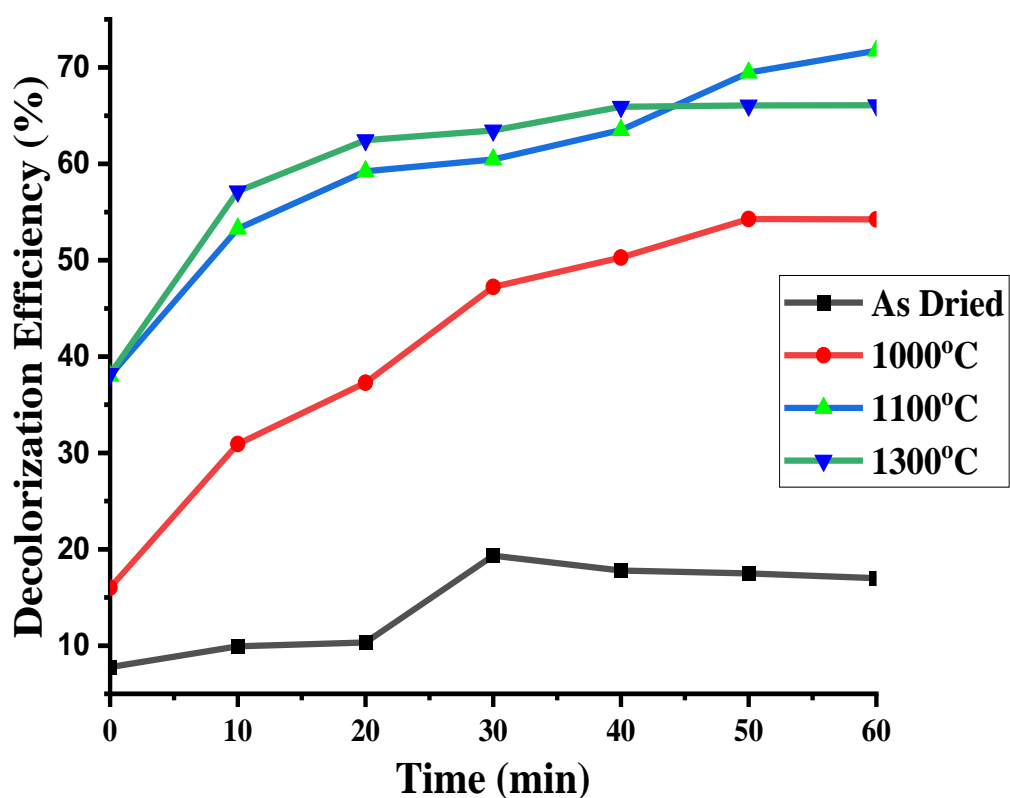
Fig 4.16: Effect of calcination temperature on decolorization efficiency vs time (min)

As dried sample showed no decolorization due to presence of silicate ion whereas highest decolorization would be shown by highest monoclinic containing sample. Though 1300ºC

temperature calcined sample showed highest monoclinic zirconia, 1100°C temperature showed highest degradation. Synthesized zirconia at 1100°C showed good percentage of monoclinic (25.5%), tetragonal (12%) and cubic (6.4%) zirconia which might be the rate controlling factor of this reaction. On the other hand, in 1300°C calcined   sample showed monoclinic structure in good amount but other zirconia structure was in very meager amount which may affect the decolorization reaction in less significantly than 1100°C sample after adsorption. Basahel and Tarek *et.   al.* [6] showed that high photocatalyst capability depend on high density of OH· which was achieved by high monoclinic ZrO_2 sample. But surface area of 1300°C nanoparticle was less than the 1100°C calcined sample. Such as the mean particle size of first one was 38.7 nm whereas mean particle size of later sample was 23.7nm.   Finer sample showed high surface area than the coarse particle as such more hydroxyle ion could be produced by 1100°C temperature sample than the 1300°C calcined sample. This is the reason behind more decolorization efficiency of 1100°C calcined sample.

Conclusion

This thesis work can be divided into following steps

- Characterization of as received local zircon sand.
- Beneficiation and characterization of upgraded zircon sand.
- Synthesis of zirconia nano powder.
- Influence of crystal structure on photocatalytic activity

5.1 Characterization of the Zircon Sand

(1)   The as received raw sand sample was mainly zircon of 73.8% pure. Main impurity was rutile (19.8%). Other impurities were based on calcium, potassium etc.

(2)   The density of raw sample was 3.41.0gm/ml. The density of dark brown to green zircon varies from 3.9-4.1 gm/ml. The lowering of density was due to presence of impurity like rutile, Calcium Cetana Silicate etc.   .

(3)   The as received zircon phase was tetragonal. No phase change was found up to $750^{o}C$ temperature in raw sand sample.

(4)   Hexagonal, spheroid, elliptical, cylindrical particles were observed under SEM. The largest particle was measured 272µm and smallest was 105 µm.

(5)   Inclusions were found in zircon particle. Zoned zircon was also observed under polarizing microscopic view which may be due to recrystallization or environmental corrosion effect.

5.2 Beneficiation and Characterization of the Zircon Sand

(1)   By acid leaching zircon yield reached 84.2% and by basic leaching the yield increased up to 86.3%. The main impurity 19.8% rutile was removed completely after acid leaching.

(2)   SEM and EDX result also showed complete elemental Ti removal. As received sample showed 5.47% Ti which was completely removed after acid leach. Elemental Zr yield increased 37.96% after basic leaching from 34.64%. in as received.

5.3 Synthesis of Zirconia Nano Powder

(1)   Dry ball milling of upgraded zircon sand up to 30 hours did not show any phase change of tetragonal zircon.

(2)   Particle size reduced from 272μm to 51.04 nm after 30 hours of ball milling

(3)   Microstrain increased with decreasing of particle size in case of nanoparticle.

(4)   Alkali fusion of zircon nano-powder with NaOH (1**:**2) at 700°C for 3 hours followed by co-precipitation with HCl and NH_4OH were used to synthesize zirconia nanoparticle.

(5)   As dried sample showed only 36.63% crystallinity among this 85% was hexagonal zircon, 8.3% tetragonal zircon and rest is quartz.

(6)   Different calcination temperatures were maintained to obtain different crystal structure of zirconia. With increasing temperature crystallinity was found to be increased.

(7)   Calcined at 800°C temperature showed predomination of tetragonal zirconia (59.6%). 21.6% was hexagonal zircon and quartz was18.8%

(8)   Calcined temperature 1000°C sample showed maximum tetragonal zirconia (78.7%). Cubic and monoclinic zirconia was 6.4% and 2.6% respectively. Undecomposed zircon found its original phase tetragonal zircon (12.1%).

(9)   1100°C calcined temperature showed maximum monoclinic zirconia (25.5%). Tetragonal and cubic zirconia formed 12.0% and 6.4% respectively. Undecomposed zircon was 55.1%.

(10)   Calcined temperature at 1300°C showed predomination of monoclinic structure (38.4%). Cubic zirconia is negligible in amount (.5%). Zirconia in tetragonal phase was 21.5%. Undecomposed zircon found 57.3% with tetragonal phase.

(11)   With increase of calcination temperature crystallinity increase. Undecomposed zircon at low temperature showed hexagonal structure. But with increase of temperature and crystallinity hexagonal zircon transformed to tetragonal zircon.

(12)   At low calcination temperature tetragonal zirconia and at high temperature monoclinic zirconia was found to be predominated. Cubic structure formed in negligible amount.

5.4 Identification of photocatalytic activity of Zirconia

(1)   Synthesized zirconia showed photocatalytic activity. Photocatalytic activity varied with different crystal structure of zirconia.

(2)   With increase of calcined temperature monoclinic structure yield increase thus increase decolorization efficiency or photocatalytic degradation.

(3)   Calcined sample at 1100°C showed maximum decolorization efficiency (71.75%) as it contained a good combination of monoclinic, tetragonal and cubic zirconia.

5.5 Summary

In this work, zircon sand was collected from Cox's Bazar beach and was characterized on the basis of parameters including composition, size, density, moisture content, crystallinity etc. Beneficiary technique like acid and alkali leach were applied to upgrade the sample. After acid and base leach 86.3% purity of zircon have been achieved by removing 19.8% rutile which was the main impurity. 30 hours dry ball mill could successfully achieve nanoparticle of zircon with particle size 51.07nm. ZrO_2 nanoparticle can be synthesized successfully by consecutive alkali fusion, co-precipitation and calcination. Depending on calcination temperature different phases were predominating like tetragonal and monoclinic. Calcined at higher temperature at 1100°C and 1300°C most of the zirconia was monoclinic in phase. But at lower temperature 800°C and 1000°C most of the zirconia was tetragonal in nature. As dried sample showed little or almost no photocatalytic activity due to presence of negligible amount of zirconia. With increase of monoclinic zirconia,

photocatalytic activity was found to be increased. Maximum decolorization was achieved by 1100°C calcined sample as it contained a combination of cubic, monoclinic and tetragonal zirconia. Synthesized zirconia from local beach sand can be used as photocatalytic degradation of textile dye of Bangladesh.

5.6 Recommendation for Further Work

The aim of the study was to find a synthesized zirconia nano powder from available zircon sand and to develop techniques for purification of zircon sand deposit.

By varying the parameters like time, temperature, stirring etc percentage of zircon yield from local zircon sand can be optimized. Furthermore, systematic investigation may be performed within the country to study the photocatalytic activity of synthesized zirconia in textile dye industry.

References

1. Yamagata, Chieko; Andrade, João B.; Ussui, Valter; de Lima, Nelson Batista; Paschoal, José O.A., "*High Purity Zirconia and Silica Powders via Wet Process Alkali Fusion of Zircon Sand,*" Materials Science Forum, Switzerland, vol. 591-593, pp. 771-776, 2008.

2. Gazi, Md. Yousuf; Tafhim; Khandakar Tahmida, "*Investigation of heavy-mineral deposits using multispectral satellite imaginary in the eastern coastal margin of Bangladesh,*" Earth Sciences Malaysia, *IDEAS*, vol. 3, pp. 16-22,2019.

3. M. Lestari; N. Dwi; N.Rizka;M. Nibras Fuadi; T.Pratapa; Suminar, "*Synthesis of high-purity zircon, zirconia, and silica nano-powders from local zircon sand,*" Ceramics International, Indonesia, vol. 45, pp. 6639-6647, 2019.

4. Hu, Cheng; Sun, Jianxun; Long, Cheng; Wu, Lina; Zhou, Changchun; Zhang, Xingdong, "*Synthesis of nano zirconium oxide and its application in dentistry,*" Nanotechnology Reviews, vol. 8 (1), pp. 396-404, 2019.

5. PR.Rauta; P.Manivasakan; V.Rajendran, "***Phase transformation of ZrO$_2$ nanoparticles produced from zircon*,**" Phase transitions, vol 85 (1-2), pp.13-26, 2012.

6. Basahel, Sulaiman N; Ali, Tarek, T; Mokhtar, Mohamed; Narasimharao, Katabathini, "*Influence of crystal structure of nanosized ZrO2 on photocatalytic degradation of methyl orange,*" Nanoscale Research Letters, vol. 10 (1), pp.73, 2015.

7. Afrin, S.; Rahman, H., "*The degradation of textile dyes using the effective bacterial consortium*,"Hylion, vol. 7(10), e08102, 2021.

8. Edwards, A.; Carranza, Z.; J. J. Kasper, "*Beach sand composition and provenance in a sector of the southwestern Mexican Pacific*," Revista Mexicana de Ciencias Geológicas, Universidad Nacional Autonoma de Mexico, vol. 26, pp. 433-447, 2009.

9. Pirkle, F. L.; Podmeyer, D. A.,"*Zircon:origin and uses*," Transactions of the Society for Mining, Metallurgy, and Exploration Inc., 1993 Transactions, vol. 292, pp. 1-19, 1993.

10. https://www.zircon-association.org/zircon-sand.html
Accessed: 05.02.2021

11. Routray; Sunita, Rao; Raghupatruni, Bhima, "*Beneficiation and characterization of detrital zircons from beach sand and red sediments in India,*" Journal of Minerals and Materials Characterization and Engineering, vol. 10, pp. 1409-1428, 2011.

12. Ahmed, M.; M, Das; S. K., Haydar; M. A., Bhuiyan; M.I, Paul, "*Study of natural radioactivity and radiological hazard of sand, sediment, and soil samples from Inani beach, Cox's Bazar, Bangladesh*," Journal of Nuclear and Particle Physics, Scientific and Academic Publishing, vol. 4, pp. 69-78, 2019.

13. T. Vaczi. (2009) "*Mineralogical studies on zircon*", project on real structure of radiation-damaged materials.

14. Finch, R. J., "*Structure and Chemistry of Zircon and Zircon-Group Minerals,*" *Reviews in Mineralogy and Geochemistry*, vol. 53 (1), pp. 1-25, 2003.

15. Zaman, M. Mashrur; Antao, Sytle M., "*Crystal Chemistry and Structural Variations for Zircon Samples from Various Localities,*" Minerals, vol.10 (11), p. 947,2020.

16. http://www.cas.miamioh.edu/~jaegerh/zircon.htm dt
    Accessed :30 Feb 2021

17. L.O. Asuquo; E. N. Bassey; A.P. Ihom, "*Characteristics of Zircon Sand and the Effect on Foundry Casting*," Journal of Mechanics and Industry Research, pp. 27-32, 2013.

18. https://www.zircon-association.org/applications.html#chemical
    Accessed :11 Dec 2021

19. MI Miah, "*A Study on Heavy Minerals Reserve and Separation Processes from Raw Beach Sands along the Coastal Belt of Bangladesh*," International Conference on Mechanical, Industrial and Materials Engineering,pp.1-3,2013.

20. https://en.banglapedia.org/index.php/Zircon
    Accessed :12 Dec 2021

21. https://en.wikipedia.org/wiki/Zirconium_dioxide
    Accessed :10 Dec 2021

22. Brog, JP.; Chanez, CL.; Crochet, A.; Fromm, Katharina M., "P*olymorphism, what it is and how to identify it: a systematic review, *"RSC Advances, vol. 3 (38), pp 12-21, 2013.

23. Vagkopoulou, T.; Koutayas, SO.; Koidis, P, "*Zirconia in Dentistry: Part 1. Discovering the Nature of an Upcoming Bioceramic,* "European Journal, 2009.

24. https://matmatch.com/learn/material/zirconium-dioxide-zirconia
    Accessed: 03 Dec 2021.

25. Madfa, A.; Al-Sanabani, Fadhel A.; Al-Qudami, Nasser H.; Al-Sanabani, Jabr S.; Amran, Abdullah G., "*Use of Zirconia in Dentistry: An Overview,*" The Open Biomaterials Journal, vol. 5 (1), pp.1-7,2014.

26. Rylski, Adam; Siczek, Krzysztof, "*The Effect of Addition of Nanoparticles, Especially ZrO2-Based, on Tribological Behavior of Lubricants*," Lubricants, vol. 8(3), p. 23,2020.

27. ÁD., Tóth; ÁI Szabó, R Kuti, "*Tribological properties of nano-sized ZrO2 ceramic particles in automotive lubricant,*" FME transection, vol.49 (1), pp. 36-43, 2021.

28. David, Clarke; Simon, Phillpot, "*Thermal barrier coating materials,*" *Materials Today*, vol. 8 (6), pp.22-29, 2005.

29. MG Gok, G Goller, "*State of the art of gadolinium zirconate based thermal barrier coatings: Design, processing and characterization*," Chapter: Methods for Film Synthesis and Coating Procedure, 2019.

30. C., Piconi; G., Maccauro, "Zirconia as a ceramic biomaterial", vol. 20 (1), pp. 1-25, 1999.

31. I. Jabber; T., Mohammed, "*Effect of Adding Nano Alumina on the Grain Size and the Mechanical Properties of Yttria-Stabilized Tetragonal Zirconia Polycrystals (Y-TZP),*" International Journal of Mechanical and Mechatronics Engineering, vol. 17 (4), pp. 86-99, 2017.

32. Amol, N.A.; Trupti, P.; Suresh, G.*;* Khanderao, P., "*A review on plant Extract Mediated Green Synthesis of Zirconia Nanoparticles and their Miscellaneous Applications*," Journal of Chemical Reviews, vol. 1(3), pp.154-163,2019.

33. The "*Zirconium Market - Growth, Trends, and Forecast (2020 - 2025)"* Dublin, Nov. 20, 2020 (GLOBE NEWSWIRE).

34. Kurny, "*Principles of Extraction of Metals*" (Unpublished Manuscript), 2006

35. https://en.wikipedia.org/wiki/Pyrometallurgy
    Accessed: 03 Mar 2022.

36. Free, Michael; Moats, Michael; Houlachi, Georges," *Electrometallurgy - Now and in the Future,*" Electrometallurgy, pp. 1-27,2012.

37. Gunarathne, V.; Rajapaksha; Anushka U.; Vithanage, M.; Alessi, Daniel S.; Selvasembian, R.; Naushad, Mu.; You, S.;Yong, S., "*Hydrometallurgical processes for heavy metals recovery from industrial sludges*, " Critical Reviews in Environmental Science and Technology,pp.1-41,2020.

38. https://www.cdc.gov/niosh/topics/nanotech/default.html
    Accessed: 04 Mar 2022

39. Anna, Giulia; Cattaneo, Rosalba; Gornati, Enrico; Sabbioni, Maurizio; Chiriva-Internati, Everardo, Cobos; Marjorie, R Jenkins ;Giovanni, Bernardini, "*Nanotechnology and human health: risks and benefits*," Journal of Applied Toxicology, vol. 30(8), pp730-744, 2010.

40. https://www.nanowerk.com/what-are-nanomaterials.php

    Accessed: 02 Feb 2022

41. Khan, Ibrahim; Saeed, Khalid; Khan, Idrees, "*Nanoparticles: Properties, applications and toxicities*," Arabian Journal of Chemistry, pp. 1-24 2017.

42. Sunita Patil and Rajkuberan Chandrasekaran, "Biogenic nanoparticles: a comprehensive perspective in synthesis, characterization, application and its challenges," *Journal of Genetic Engineering and Biotechnology* vol. 18(67),2020.

43. Cristina, Raab, "*Production of nanoparticle and nanomaterials*," Institute of Technology Assessment of Australian Academy of Science, 006en, 2015.

44. E. V. Dudnik, "*Modern methods for hydrothermal synthesis of zirconia nanoparticle*," Powder Metallurgy and Metal Ceramics, vol. 48 (49), pp. 238-248, 2009.

45. A. V. Shevchenko; A. K. Ruban; E. V. Dudnik; V. A. Mel'nikova, "*Hydrothermal synthesis of ultrafine zirconia powders,*" Powder Metallurgy and Metal Ceramics, vol. 36 (7),pp. 420-424,1997.

46. https://www.911metallurgist.com/making-zirconia/
    Accessed: 05 Feb 2022

47. Poernomo, H; Sajima, ; Pusporini, N D.," *Synthesis of Zirconium Oxychloride and Zirconia Low TENORM by Zircon Sand from Landak West Kalimantan*," Journal of Physics Conference Series, vol. 1436 (1), p. 012106,2020.

48. P., Leture; M., Prassas ; A., Lecomte; A., Dauger, "*Low temperature synthesis of Zircon by sol-gel process*," the Sol-gel gateway, 2001.

49. AK Aboul-Gheit, DS El-Desouki, SM Abdel-Hamid "*Sulfated zirconia catalysts for low temperature isomerization of n-pentane,*" Egyptian Journal of Chemistry, vol. 55(5), pp. 509-527,2012**.**

50. N.A Mohammed; A.M Daher, "*Preparation of High-Purity Zirconia from Zircon: An Anion-Exchange Purification Process*", Hydrometallurgy, vol.65(2-3), pp. 103 107, 2002.

51. Reginaldo José Farias da Silva; Achilles Junqueira Bourdot Dutra; Julio Carlos Afonso, "*Alkali fusion followed by a two-step leaching of a Brazilian zircon concentrate,* Hydrometallurgy," vol.117-118, pp. 93-100, 2012.

52. Długosz, Olga; Szostak, Krzysztof; Banach, Marcin, "*Photocatalytic properties of zirconium oxide–zinc oxide nanoparticles synthesized using microwave irradiation,*" Applied Nanoscience, 2019.

53. Prihod'ko, Roman V.; Soboleva, Nely M., "*Photocatalysis: Oxidative Processes in Water Treatment,*" E-Journal of Chemistry, vol. 2013, pp.1-3,2013.

54. Tee, Si Yin; Win, Khin Yin; Teo, Wee Siang; Koh, Leng-Duei, "*Recent Progress in Energy-Driven Water Splitting,*" Advanced Science, 2017.

55. Anbalagan, S.; Ponnusamy, K., "*Photocatalysis for removal of environmental pollutants and fuel production: a review,*" Environmental Chemistry Letters, 2020.

56. Naher, Sumsun; Haseeb, A. S. M. A. "*Production and purification of zircon opacifier from zircon found in the coastal area of Bangladesh.*" Journal of Materials Processing Technology, Elsevier, vol. 205, pp. 203-206, 2008.

57. Michel-Levy,A.; Lacroix, A., (1988) Les minerauxdes roches. Librairie Polytechnique, Paris.

58. Bjorn, E. S., "*A revised Michel-Levy Interference Colour Chart Based on First-Principles Calculations,*" European J. Minerology, vol. 25, pp. 5-10,2013.

59. Tania., 2014, "*Upgradation of Locally Available Silica from the Production of Solar Grade Silicon,*" Bangladesh University of Engineering and Technology.

60. https://www.surfacesciencewestern.com/analytical-services/scanning-electron-microscopy-coupled-with-energy-dispersive-x-ray-semedx-spectroscopy/ Accessed: 01 Jan 2022.

61. https://www.twi-global.com/technical-knowledge/faqs/x-ray-diffraction Accessed: 01 Jan 2022.

62. https://www.smacgigworld.com/blog/principle-uv-vis-spectroscopy-.php

Accessed: 04Jan 2022.

63. Saravanan, M. S. Senthil; Sivaprasad, K.; Babu, S. P. Kumaresh; Susila, P.; Murty, B. S.; Giri, P. K.; Goswami, D. K.; Perumal, A.; Chattopadhyay, A, "*Synthesis and Characterization of CNT Reinforced AA4032 Nanocomposites by High Energy Ball Milling*," International Conference on Advance Nanomaterial and Nanotechnology, pp. 82-87, Assam, India, 2010.

64. Kasatkin, F Girgsdies, "*HRTEM Observation of the Monoclinic-to-Tetragonal (m-t) Phase Transition in Nanocrystalline ZrO₂*," Journal of Materials Science, vol. 39, 2151–2157,2004.

65. K. W., Chau; Y. C., Yang ; P. H., Geil , "*Tetragonal → twinned hexagonal crystal phase transformation in polybutene-1*," Journal of Materials Science , vol. 21, pp. 3002–3014, 1986.

66. Gulshan, 2009, "*Simultaneous ion uptake properties and photoactive properties of alumina-iron oxide compounds prepared by solution methods*", Tokyo Institute of Technolog, Japan.

67. JA, Navio; MC, Hidalgo; SG, Botta; MI, Litter - Langmuir, "*Preparation and Physicochemical Properties of ZrO2 and Fe/ZrO₂ Prepared by a Sol−Gel Technique*," *American Chemical Society*, Vol 17, pp. 202-210, 2001.